1.0 Introduction

The use of active control surfaces to enhance the control of aircraft has become a prevalent technique throughout the aerospace industry. Active control surfaces refer to the use of the movements of the control surfaces on the wing, or even the twisting of the wing itself, to control the aircraft. Phenomena such as Limited Cycle Oscillation and control reversal at high airspeed are current problems plaguing modern aircraft; the use of active control surfaces has the potential to be the solution. Furthermore, implementing active control surfaces have been shown to increase the maximum lift coefficient of an aircraft beyond conventional values. However, before active controls can be commercialized into real aircraft, scaled models must be used to optimize their effectiveness. Wind tunnel tests of actively controlled wing-stabilator models are instrumental to designing an effective active control system for mass production.

1.1 Project Goals

The project goal of the design team at Active Wing Technologies (AWT) was to restore the wing-stabilator model, shown in figure 1, to working order and to modify the model for use in studies requiring active control surfaces. The active wing group of the spring 2002 semester recovered the wing-stabilator model from storage minus the stabilator. The immediate goal of AWT was to rebuild the lost stabilator. However, the decision was made to put the task of rebuilding the stabilator in abeyance until the design of the modified stabilator was finalized.

Figure 1. Current Wing-Stabilator Model [1]

The active wing group of spring ‘02 focused research on current technological fields of interest in which a working active wing-stabilator model would be of use; they provided a solid foundation of information in the areas of LCO and control reversal. AWT has expounded upon the work of the spring ’02 active wing group. First, in working towards constructing a functional active wing, a step back was taken to investigate the details of how the original active wing model worked. The concepts of the original design were used in attempting to implement current technology. Research conducted on implementation schemes of active control surfaces were the basis on which ideas for implementing control surfaces in our model were formed. Furthermore, studies have been conducted on possible actuator power supplies that could be used to move a control surface in the current wing-stabilator model. Cost-Benefit analysis was preformed to help decide the optimum power supply to control the active control surfaces. Last, progress has been made in the area of control electronics. AWT has shown that the use of

analog control systems is still feasible in the active wing project. However, a digital control system would be optimal to implement complex control theory.

The responsibilities of the project were divided into three equal parts as follows: Basil Philip doubles as team leader and the investigator of active control surface implementation; Naoki Sato is in charge of studies on the optimal actuator power supply and research on increasing the maximum lift coefficient; and David Fuentes heads the control system research.

2.0 Design Project Background

The foundation for our project was the work done by the active wing group of spring 2002 and the 1978 master's thesis project by Randall Bolding. A compendium of the work done by Bolding and the spring '02 active wing group is given in this section.

2.1 Suppression of Flutter Utilizing Actively Controlled Stabilator

The 1978 master's thesis by Randall Bolding is the origins of the active wing design project. Half of the wing-stabilator model built by Bolding is currently in the possession of AWT. Bolding's primary use of the wing-stabilator model was to research the use of the stabilator as an active control to suppress flutter. The design team at AWT sought to further Bolding's work. Bolding's master's thesis has been read multiple times in an attempt to understand the fundamental principles behind the wing-stabilator model. In particular, the hydraulic power supply and the analog control system have been researched thoroughly. However, the graduate level details, such as the formulation of the control laws that were utilized to suppress flutter, were not given much attention. It is important to note that, Bolding used the interaction between the flow about the wing and the stabilator to suppress flutter; the stabilator was the active control. In AWT's current project, control surfaces are considered the active controls.

2.2 Active Aeroelastic Wing

One of the main focuses of the spring '02 active wing group was to study the applications of the actively controlled wing-stabilator model in the field of the Active Aeroelastic Wing. The concept behind the Active Aeroelastic Wing stems from the problem of control reversal at high airspeeds. To summarize, at large airspeeds, latent aerodynamic forces negatively affect the actions of an aircraft's control surfaces. As an

example, consider the normal operating conditions of an airplane during rolling motion. At normal cruise conditions one aileron is deflected up and the other is deflected down, causing the aircraft to roll. The aircraft rolls because of an imbalance of forces on the wings of the aircraft; the up aileron decreases the camber of one wing, which decreases the lift; the down aileron increases the camber of the other wing, which increases the lift. Accompanying the change in lifting forces is an axial torsion moment about each of the wings. The torsional moment about the wing with the up aileron acts to increase the angle of attack of the wing thus increasing the lift force; the torsional moment about the wing with the down aileron acts to decrease the angle of attack thus decreasing the lift force. The end effect is that the latent aerodynamic forces undermine the effectiveness of the aileron. Moreover, the latent aerodynamic forces that result in the unwanted torsional moment increase with airspeed. A critical airspeed exists at which deflecting the ailerons are useless; furthermore, beyond this critical airspeed the latent aerodynamic forces are so pronounced that the deflection of the ailerons produces the opposite effect from its intent. The idea behind Active Aeroelastic Wing technology is to utilize the unwanted torsional moment and turn it into a positive desired effect. Active Aeroelastic Wing technology uses active control surfaces, such as the outboard leading edge flaps and the ailerons, to utilize the aerodynamic forces on the twisted wing to control the aircraft. Further details are left to the final report of the spring ’02 active wing group [2].

2.3 Limited Cycle Oscillation

Limited cycle oscillation (LCO) is an unpredictable aerospace phenomenon because it is induced by a variety of flight conditions of the aircraft. LCO causes the wings of the aircraft to oscillate with limited amplitude in the vertical plane. LCO does

not destroy an aircraft; however, it induces fatigue into the structure and eventually causes failure. Furthermore, LCO causes uncomfortable flying conditions for the pilot and could even inhibit the ability of the pilot to accomplish his mission. The phenomenon of limited cycle oscillation is not to be confused with classic flutter. The defining difference between LCO and classic flutter is LCO's limited-amplitude characteristic. In classic flutter, the amplitude of the wing oscillation diverges to infinity with catastrophic effects; however in LCO, the wing oscillation is finite in amplitude. The amplitude of the oscillation is limited by an unidentifiable non-linear mechanism. Figure 2 compares the bounded nature of the amplitude of the wing tip oscillation for LCO, and the divergent nature of classic flutter. Since, the mechanism that leads to the onset of LCO is not well understood; we cannot accurately predict its occurrence. The system identification toolbox in Matlab will be instrumental in developing a mathematical model of the defining equations of motion of LCO. Once a mathematical model of LCO is determined, engineers will be able to predict its occurrence.

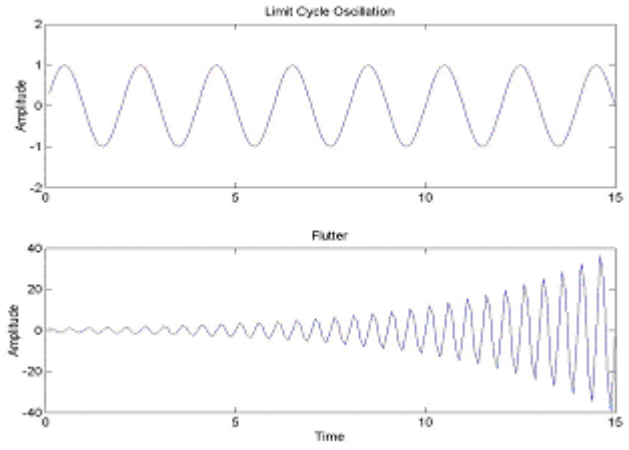

Figure 2. Displacement of LCOs and Flutter [2]

2.4 System Identification of an Arbitrary Process

The purpose of system identification is to construct a mathematical model of the defining equations of motion of any system based on experimental data. When a system is identified, the simulated response of the mathematical model is equal to the response of the real-life system. Figure 3 shows an outline of the system identification process. The system identification toolbox in Matlab is programmed to output a mathematical model of the process given experimental data of the output in response to a given input. Through an iterative process, Matlab determines the equations of motion representative of the true system. The same input is given to a *true system* and a *model system.* The error is the difference in the response between the true system and the modeled system for the same input. When the error approaches zero, the system has been identified. The identification of a complex system requires a numerical method, like the one utilized by Matlab, to determine the equations of motion. However, in some cases the system is simple enough that the equations of motion can be obtained analytically.

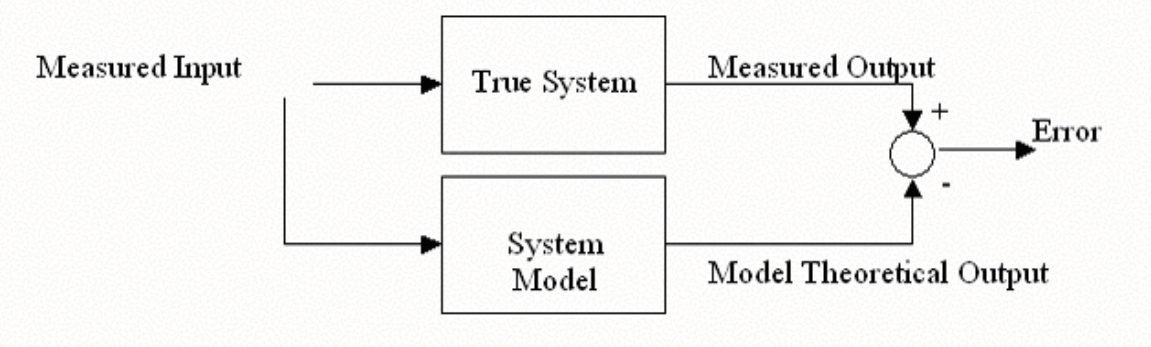

Figure 3. System ID Process [2]

3.0 Increasing the Lift Coefficient

In addition to utilizing active control surfaces to control LCO and control reversal, AWT has researched active control surfaces for the use in increasing the maximum lift coefficient of an aircraft. The desire to increase the maximum lift coefficient stems from the desire to decrease the stall speed of the aircraft. Typically, the minimum airspeed of an aircraft is limited by the stall speed. As the aircraft approaches the stall angle, the airflow over the top of the wing detaches. The detached flow leads to a drastic loss in lift causing the aircraft stalls. The stall speed is expressed by the following equation

$$V_{stall} = \sqrt{\frac{2W}{S\rho C_{L\max}}} \qquad [3.0.1]$$

The weight of the aircraft is given by W; the planform area of the wing is given by S; ρ is the density of the air; and $C_{L\max}$ is the maximum lift coefficient of the airfoil. In most cases, the density of the air is constant with altitude and the planform area of the wing is as small as possible to minimize the weight. The maximum lift coefficient, $C_{L\max}$, is the ideal parameter to optimize in order to reduce stall speed. This section discusses how $C_{L\max}$ can be increased by controlling the airflow about the wing. Leading and trailing-edge flaps and leading edge slats are the traditional way to increase the lift coefficient. Oscillating flaps are new technique to used to achieve higher lift coefficients.

3.1 Leading-Edge Devices

Nose flaps, Kruger flaps, and slats are several types of leading edge devices used to increase the maximum lift coefficient of the aircraft. A slat is shown figure 4. The system has an opening at the leading edge of the airfoil allowing high pressure air under

the airfoil to pass. As a result, the high pressure air mixes with the air at the top surface, and increases the energy of the boundary layer at the surface. "By increasing the energy of the boundary layer the wing can sustain higher angles of attack and a higher maximum coefficient of lift." [3]

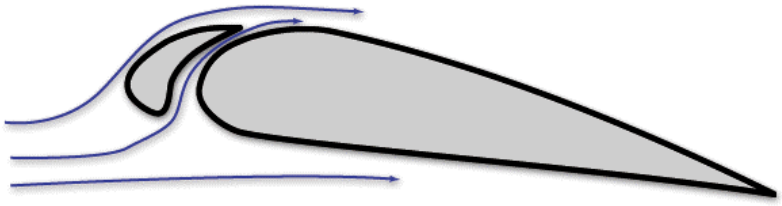

Figure 4 Leading Edge Wing Slat [4]

3.2 Trailing Edge Flaps

Flaps change the pressure distribution around the airfoil by changing its chord length and camber. There are several types of trailing edge flaps. A plain flap is the most common type of flap. When flaps are deflected downward, they increase chord length, planform area, and camber of the airfoil. As shown in equation 3.0.1, increasing the planform area of the airfoil results in a decrease in stall speed. Moreover, a cambered airfoil inherently has a higher lift coefficient.

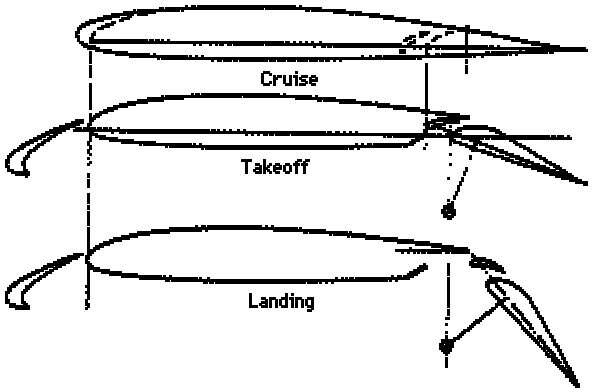

Figure 5. Double-Slotted Flap and Slat System [5]

Figure 5 shows the double slotted flaps mounted on a wing. Slotted flap systems are used to achieve higher maximum lift coefficient than the plain flap system. "Slotted flaps achieve higher lift coefficients than plain or split flaps because the boundary layer that forms over the flap starts at the flap leading edge and is *healthier* than it would have been if it had traversed the entire forward part of the airfoil before reaching the flap [5]."

3.3 Oscillation excitation

The oscillating flap is usually located near the leading edge of the wing to control the separation of the airflow from the wing. As mentioned before, the separation of the airflow induces stall. The purpose of the oscillating flap is to delay the separation or reattach the separated flow onto the surface. The fact that separation occurs at the top surface of the wing means that the airflow does not have enough energy to withstand the adverse pressure gradients. The loss of energy of the flow can be overcome by vortices created by the oscillating flap. Vortices are energetic rotating fluid cells. Studies have found that "the vortices shed from the oscillating flap enhance the momentum transfer between the free stream and the boundary layer, which makes the reattachment of vertices occur more upstream [6]." The further upstream the vertices are, higher maximum lift coefficient can be achieved. Moreover, the maximum lift coefficient was further increased when the excitation frequency of the flap corresponds to the vortex shedding frequency [6].

The applications of the oscillating flaps have been shown to be effective in controlling the separated airflow over the wing and increasing the maximum lift coefficient at certain excitation frequencies. However, there still are problems for this technique; there is no conclusive result as regards to the oscillating mode shapes of the

flap motion. Furthermore, this technique is only successful for limited airflow conditions. AWT believes that further studies of increasing the lift coefficient by oscillating a flap are in order. Bolding's wing-stabilator model can be modified for simultaneous studies in LCO suppression, control reversal, and increasing the lift coefficient. The implementation of active control surfaces into the current wing-stabilator model applies to all three areas.

4.0 Active Control Surface Implementation for Studies on LCO

This section was included to provide a basis for designing active control surfaces to be used in the current wing-stabilator model of AWT. As a first step in the implementation process of active control surfaces for LCO, AWT will review active control surfaces used to suppress flutter. Despite the fact that flutter and LCO are caused by different reasons, AWT feels that the study of active control surfaces used to suppress flutter is a good place to start because the goal for both orientations is to prohibit wing tip oscillation. The implementation schemes of active control surfaces from *NASA TR R-450* [7] are analyzed in this section. The concepts of the implementation scheme will then be viewed in a form applicable to the current wing/stabilator model.

4.1 Flutter Suppression by Use of Active Control Surfaces

At NASA Langley Research Center in Hampton, VA, a team of engineers sought to suppress flutter by means of using active controls. Flutter is the self-excited oscillation in which energy is absorbed by the lifting surface from the airstream [2]. El Nissim's aerodynamic energy criterion [8] states that sign of the work per cycle done by the system on the airstream, when the lifting surface undergoes an oscillatory motion, indicates the state of stability of the system. Nissim stated that a necessary and sufficient condition for the prevention of flutter is for all oscillatory motions of an elastic system in an airstream to have positive work done by the system on the surrounding airstream. A brief discussion concerning key points illustrated by equations given by Nissim, is provided below in order to grasp his concept of flutter suppression centered on aerodynamic energy considerations.

Consider the equations of motion for a system with n degrees of freedom [8]

$$\{F\} = -\omega^2 \left[[M] + \pi\rho b^4 S([A_r] + i[A_I]) \right] \{q\} + [K]\{q\} \qquad [4.1.1]$$

where, at flutter, the generalized force {F} = 0 and ω is the circular frequency of oscillation; [M] is the mass matrix; $[A_r]$ and $[A_I]$ are the real and imaginary unsteady aerodynamic-force matrices, respectively; [K] is the structural stiffness matrix; ρ is the fluid density; S and b are a reference area and length, respectively; and {q} is the generalized displacement vector.

Nissim shows that the work per cycle W done by the system on the airstream can be written as [8]

$$W = \frac{1}{2}\pi^2 \rho b^4 S \omega^2 \left[q_R - iq_I \right] [U] \{ q_r + iq_I \} \qquad [4.1.2]$$

where [8]

$$[U] = \left[-([A_I] + [A_I]^T) + i([A_R] - [A_R]^T) \right] \qquad [4.1.3]$$

A positive value for W indicates a transfer of energy from the system to the airstream and hence, stability. The matrix [U] is Hermitian and therefore possesses real eigenvalues. By use of these eigenvalues, it is shown in reference 2 that the energy input per cycle into the airstream can be reduced to a principal quadratic form as [8]

$$W = \frac{1}{2}\pi^2 \rho b^4 S \omega^2 \left[\lambda_1 (\xi_{R_1}^2 + \xi_{I_1}^2) + \lambda_2 (\xi_{R_1}^2 + \xi_{I_1}^2) + \ldots + \lambda_n (\xi_{R_n}^2 + \xi_{In}^2) \right] \qquad [4.1.4]$$

where λ_n are the eigenvalues of the matrix [U] and ξ denotes generalized coordinates associated with the aerodynamic energy. A notable characteristic of the energy method is that the criterion for flutter stability is determined by the characteristics of the aerodynamic-force matrices alone. Therefore, if a particular system has undesirable flutter characteristics such as too low of a flutter speed, the flutter characteristics can be

improved if a mechanism can be found which changes the [U] matrix in a appropriate manner. One such mechanism is the addition of active control surfaces to the basic system. The motions of these surfaces generate aerodynamic forces that modify the aerodynamic terms in the [U] matrix for the basic system. For flutter suppression, the control surface deflections are related by a control law to the plunging and pitching motion of the main surface. Nissim points out that a suitable configuration is one utilizing both leading-edge and trailing-edge controls since the two working together would provide independent control lift and pitching moment.

The wing configuration used in the analytical study of flutter suppression can be seen in figure 6. Three spanwise locations of aerodynamic control surfaces were considered in the investigation, designated as II, III, and I in the figure. Each configuration consisted of both leading-edge and trailing-edge control surfaces activated by sensors located on the wing at the 30 percent and 70 percent midspan chord of each spanwise location. The results showed improvement in flutter speed of 21 percent for configuration I, 28 percent in configuration II, and 11 percent for configuration III. The combined use of configurations II and I working concurrently produced an improvement in flutter speed in excess of 41 percent.

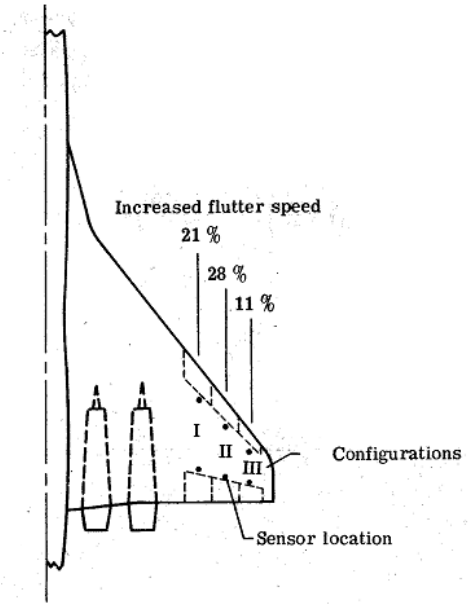

Figure 6. Calculated Effectiveness of Aerodynamic Energy Concept Flutter-Suppression Systems [7]

The analytical study indicated that active control surfaces were very effective in increasing flutter speeds; therefore, a research program was undertaken to construct a model that would incorporate the idea of control surfaces so experimental results could be compared to the analytical results. The following design was used as a start in AWT's ideas of implementing control surfaces with an actuating system and power supply.

The design objective was to have a relatively simple and inexpensive model that would be of adequate size to incorporate control surfaces with an oscillatory drive mechanism. Figures 7 and 8 show schematic illustrations of the wing model.

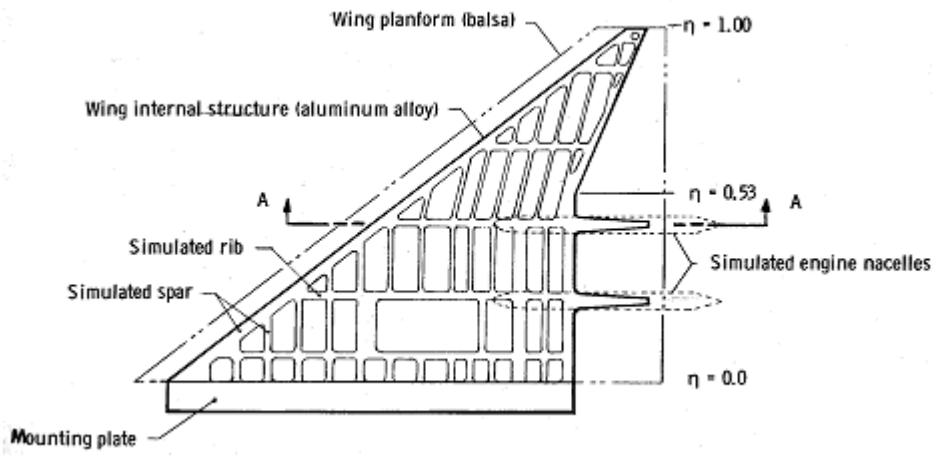

Figure 7. Typical Details of Model Construction [7]

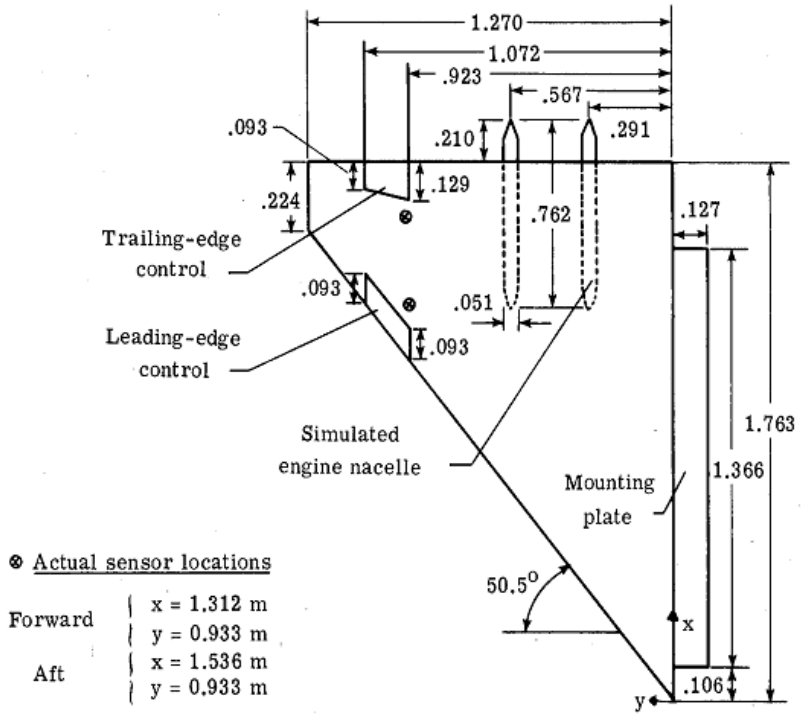

Figure 8. A Sketch of the Delta Wing Model with all Dimensions in Meters [7]

For details on the construction of the wing, see *NASA TR R-450* [7]. Initially, the control surfaces were mechanized with an electro-mechanical system. The original

mechanization consisted of a quick-response high-torque electric dc motor, mounted externally to the model, which was connected to and drove the control surface through a drive shaft. However, a problem occurred with the wind-up of the long drive shaft. After researching considerably it was decided to develop a hydraulic servo system so that the actuator could be located internally, next to the control surface. Prior to installing the new control system, a static hinge moment test was conducted in the wind tunnel. Measuring the order of magnitude of the hinge moment was valuable to finalizing the actuator design. The team had to design and fabricate special actuators to match the desired torque, small size, and lightweight requirements that the model demanded. A photograph of the actuator and its components installed in the wing can be seen in the following figure 9 below.

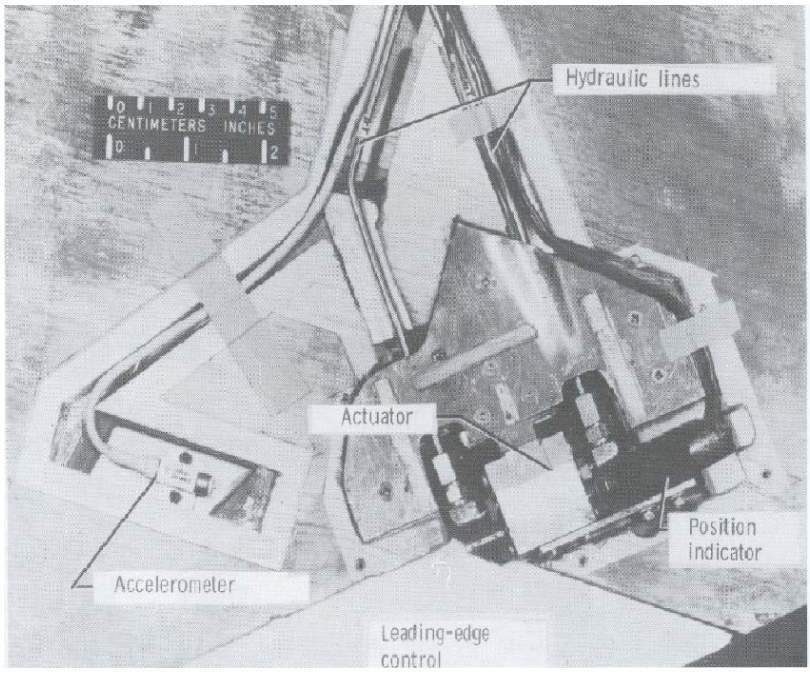

Figure 9. A Mockup of the Actuator System within the Wing [7]

The actuator consisted of a closed compartment separated into two chambers by a self-sealing vane attached to a shaft and supported by two miniature precision ball bearings.

Shaft rotation is obtained by applying a differential hydraulic pressure between the two chambers. The actuator has a mass less than 60 g and is capable of providing 4.52 N-m torque output over the frequency range from 0 to 25 Hz with a 6.9 MPa supply pressure. The actuator angular displacement capability was approximately $\pm 9.0°$. To formulate an adequate mathematical model to be used in the flutter analysis, the nine structural mode shapes, generalized masses, and natural frequencies were measured. The mode shapes were obtained by using a non-contact deflection-measuring device which is described in detail in *A Non-contacting Displacement Measuring Technique and Its Application to Current Vibration Testing* [7].

Using control law theory, an analytical study of the wing model was performed to determine the best locations for the control surfaces and motion sensors. The procedure, results, testing, and modifications of the experiment can be seen in *NASA TR R-450* [7].

With the analytical study and the experiment on flutter in mind, AWT constructed similar active controls on a program called Shade. Details of the design are offered in the next section.

4.2 Constructing Ailerons and Flaps

Figure 10 is a schematic of a possible design for implementing active controls. AWT plans to add ailerons and flaps to the existing F-111 wing model in WRW 319. The control surfaces will assist Active Wing Technologies in researching and testing for LCO data. The following schematic includes leading- and trailing-edge active controls. The trailing-edge flaps will be constructed inboard and the ailerons will be constructed outboard with trim tabs fixed on the trailing edge. Spoilers are optional and are conventionally constructed above the flaps. AWT decided to go with a leading-edge slat

as opposed to an trailing edge flap after realizing the maximum lift coefficient could be increased significantly by this convention.

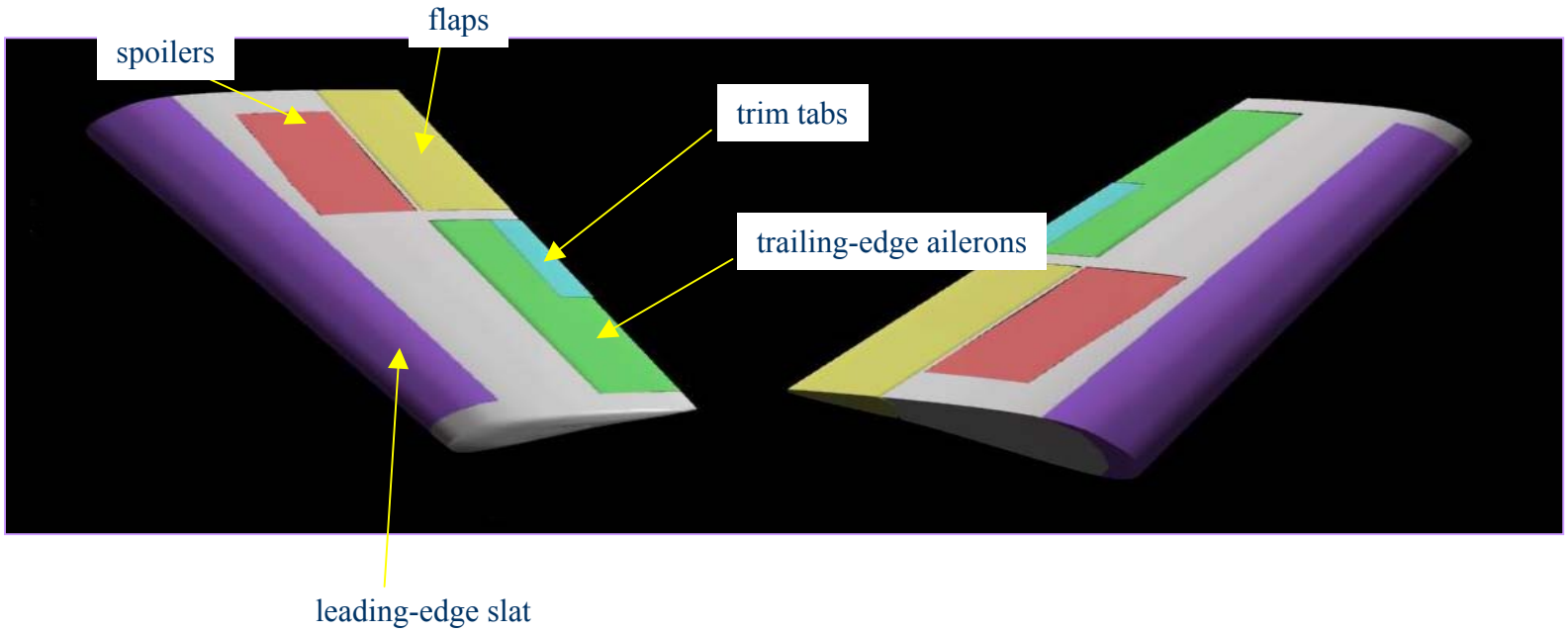

Figure 10. A Design of Active Controls by AWT

The tip of the wing model will not include control surfaces. Hydraulic actuators are possibly the means to displace the active controls. AWT was unable to decide on a power supply for the active controls but future groups can make a decision when a suitable power supply is found for the wing sweep. Small hydraulic systems were used as power supplies in the original experiment conducted by Randall Bolding in his pursuit to find a method of suppressing flutter. This is a possible system for displacing the control surfaces because a smaller hydraulic system may not pose as many issues as the hydraulic system used for the wing sweep. The wing sweep hydraulic system was much larger, outdated, and extremely loud. Modern hydraulic systems will not have such issues, especially for a much smaller power requirement. The hydraulic lines can be fed within the wing and will not interfere with wind tunnel testing. AWT plans to construct

the control surfaces by cutting into the wing model and adding the control surfaces. An alternative method for a power supply is to use a servo to displace the wing. However, the flaps and ailerons will need a rod in order to be connected to the power supply. The control surfaces will pivot about the rod and a gear system could be also of use in order to connect the flaps to the ailerons. The servos can be simultaneously connected to the wing sweep power supply if necessary. Below is a schematic of the side view of the wing model.

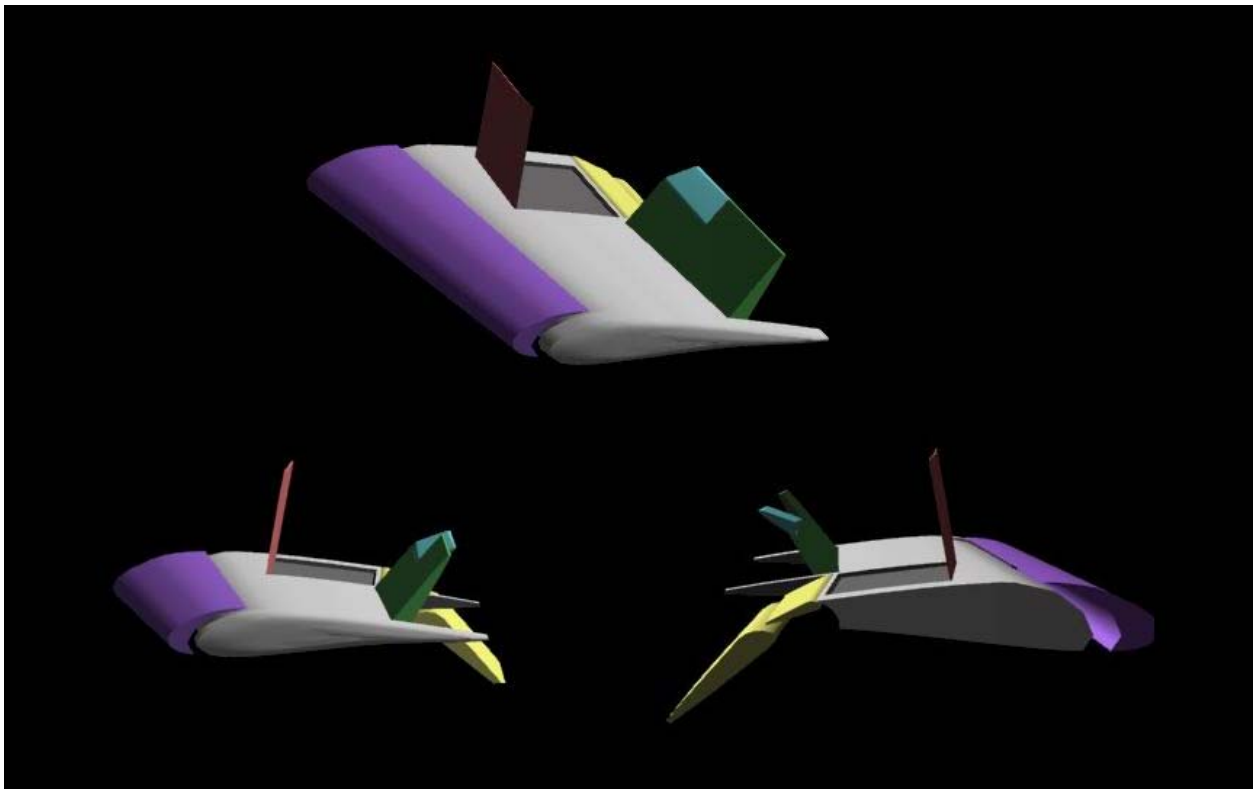

Figure 11. Control Surface Design

The design of the control surfaces was constructed from existing models used in the air force such as the F/A-18A. Figure 11 shows the range of rotation of the control surfaces about the wing. In order to find the power requirement for the actuators or servo system to be located in the wing model for the control surfaces, the moment will have to be

calculated about the control surfaces. The moment can be calculated through wind tunnel testing. This is a consideration for future groups continuing the research on LCO phenomenon.

4.3 Calculating the Hinge Moment

The following section is provided as a supplemental study of flight dynamics. This section is a starting point or a place to begin in calculating hinge data for determining power requirements and control surface specifics. The force calculations discussed in this section is of the elevator and not the flaps itself. Also, the following study pertains exclusively to the static conditions and the dynamic considerations are left for future groups. The discussion is taken from Dr. David G. Hull's *Introduction to Airplane Flight Mechanics* [9].

The air flowing over an elevator creates a pressure distribution on its surface that triggers a moment about the elevator hinge line called the elevator hinge moment. In order to maintain the elevator at a specific angle, the pilot must provide a control moment opposite in sign to the hinge moment by a force on the control column. This can be done by the use of a hydraulic system if the pilot is not able to move the elevator himself in the case of a large aircraft. Otherwise, the pilot is directly connected to the elevator so that he will be able to feel the full affect of the moment acting on the elevator and thus counteract the moment by force.

To illustrate the analysis of the stick force and hinge moment, consider the reversible control system in figure 12 system.

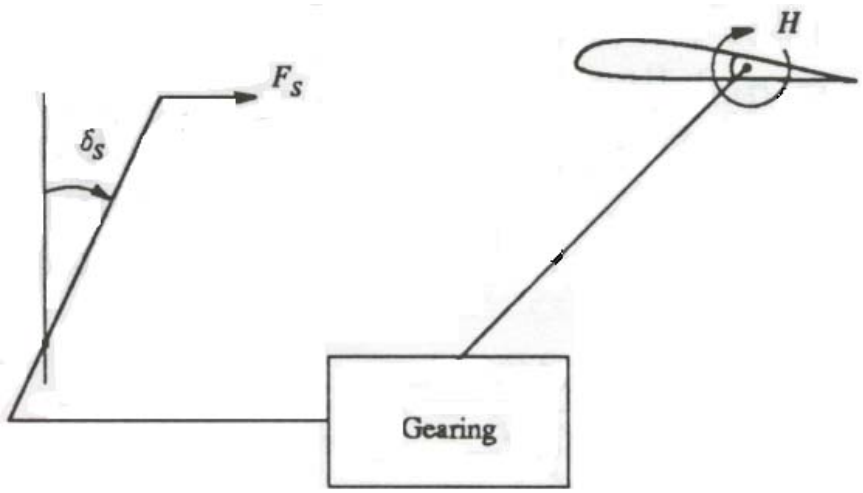

Figure 12. The Sign Convention for Control

A positive hinge moment is in the clockwise direction. The stick force can be expressed as

$$F_S=GH \qquad [4.3.1]$$

where *G* is the gearing and *H* is the hinge moment. The gearing includes the moment arm which translates the stick force to a moment. The elevator hinge moment is then changed to a coefficient by dividing by the dynamic pressure $\bar{q}_H$, the elevator area S_E, and a mean elevator chord $\bar{c}_E$ expressed as follows

$$C_H = \frac{H}{\bar{q}_H S_E \bar{c}_E} \qquad [4.3.2]$$

so that the stick force becomes

$$F_S=G\ \bar{q}_H S_E \bar{c}_E\ C_H \qquad [4.3.3]$$

Next, the hinge moment is assumed to vary linearly with α_H and δ_E so that

$$C_H = C_{Ho} + C_{H_{\alpha_H}} \alpha_H + C_{h_{\delta_E}} \delta_E \qquad [4.3.4]$$

where C_{Ho} =0 because tail surfaces are symmetric. Finally, with the tail efficiency factor, the angle of attack of the horizontal tail, the downwash angle, and equation 4.3.3, the stick force leads to the following

$$F_S = G\bar{q}\,\eta_H S_E \bar{c}_E [-C_{H_{\alpha_H}} \varepsilon_o + C_{H_{\alpha_H}}(1-\varepsilon_\alpha)\alpha + C_{H_{\alpha_H}} i_H + C_{h_{\delta_E}} \delta_E] \quad [4.3.5]$$

To isolate the dynamic pressure effect, the following expressions are used

$$\begin{aligned} \alpha &= \alpha_o + \alpha_{C_L} C_L \\ \delta_E &= \delta_{E_o} + \delta_{EC_L} C_L \end{aligned} \quad [4.3.6]$$

where $C_L = 2W/\rho S_W V^2$. Figure 13 illustrates the stick force vs. the flight speed for low sub-sonic speeds.

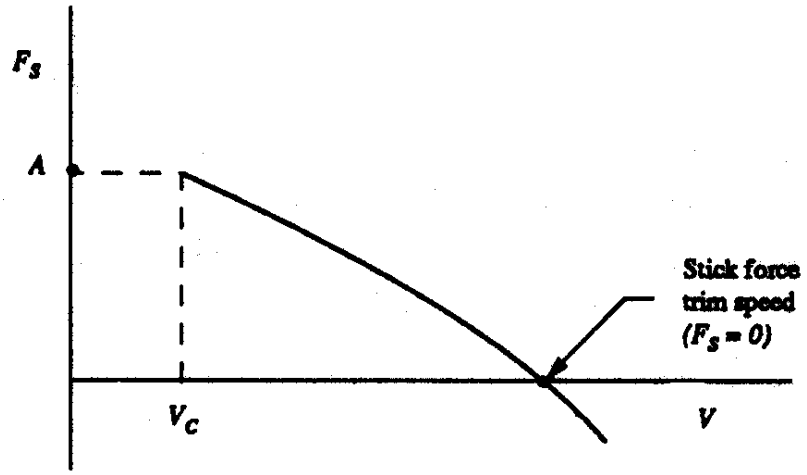

Figure 13. The Stick Force vs. the Flight Speed

5.0 Actuator Power Systems for the Wing-Stabilator Model

In this project, the purpose of the actuator is to sweep the wing, pitch the stabilator, and oscillate the control surfaces. The hydraulic actuator power system built by Bolding is no longer functional and complications have arisen in the repair of the outdated system. The decision has been made to discard the restoration of the outdated system and investigate new technology in actuator power systems. Further, Bolding's wing-stabilator model required an output force of 300 lb to sweep the wing, and maximum frequency response of 56Hz to oscillate the pitch of the stabilator. The larger frequency response range that is required to actuate active control surfaces induced concern for AWT. The concern led AWT to investigate multiple types of actuator power systems. The three types of actuator power systems considered were a modern hydraulic system, a piezoelectric system, and a magnetic shape memory based system.

5.1 Hydraulic System

A modern hydraulic power supply system was considered first as one of the possible replacements for Bolding's system. AWT's initial idea was that a modern hydraulic power supply could provide the design specifications that Bolding's outdated power supply could not. The fundamentals of the hydraulic power supply system are explained in this section along with a brief review of the hydraulic system built by Bolding.

The basic idea behind the hydraulic system is Pascal's theorem. The theorem states that when a pressure is applied to a liquid in a sealed container, the pressure is distributed across the liquid, and the pressure is the same everywhere throughout the

liquid. For example, the basic application of Pascal's theorem is explained in figure 14. Two cylinders are connected, and filled with a liquid. The cylinders differ in the cross sectional area; the ratio of the cross sectional area is 1 to 10. When a force of 10 N is applied to the left cylinder, the right cylinder experiences a force of 100 N. The piston in the right cylinder achieves a large force while a small force is applied to the piston in the left cylinder. However, it is important to note that the conservation of energy still applies. The 100 N forces acts through a shorter distance than the 10 N force.

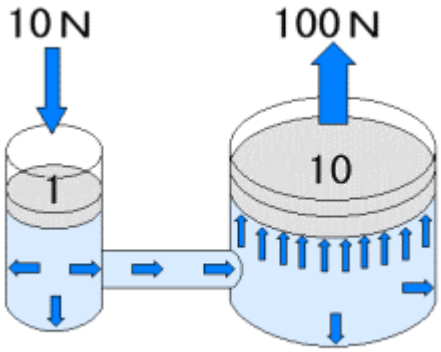

Figure 14. Pascal's Theorem [10]

Any hydraulic systems can be divided into four logical segments: a power input segment, a control valve segment, a power output segment, and a power transmission system. The first segment is the power input segment. The power input segment may be considered the power supply of the entire hydraulic system. The job of power input segment is to raise the pressure of the operating fluid in the hydraulic system. Pumps and accumulators are the common types of power source used in hydraulic systems. Pumps convert work done by rotating or translating shafts into flow energy. Accumulators convert power generated in a gaseous medium or energy stored in a gaseous or

mechanical spring into flow energy.

Any type of pump operates by allowing oil to flow into a pumping cavity and then forcing the oil out into another chamber. A gear pump is shown in Figure 15. A gear pump adds kinetic energy to the flow by turning the gears in the path of the flow. Advantages of the gear pumps are: it is a relatively simple structure, has less structural failure, and it is a small inexpensive design. Disadvantages are the noise and vibration generated, the limited pressure handling capabilities; and it cannot deal with a lot of amount of oil flow.

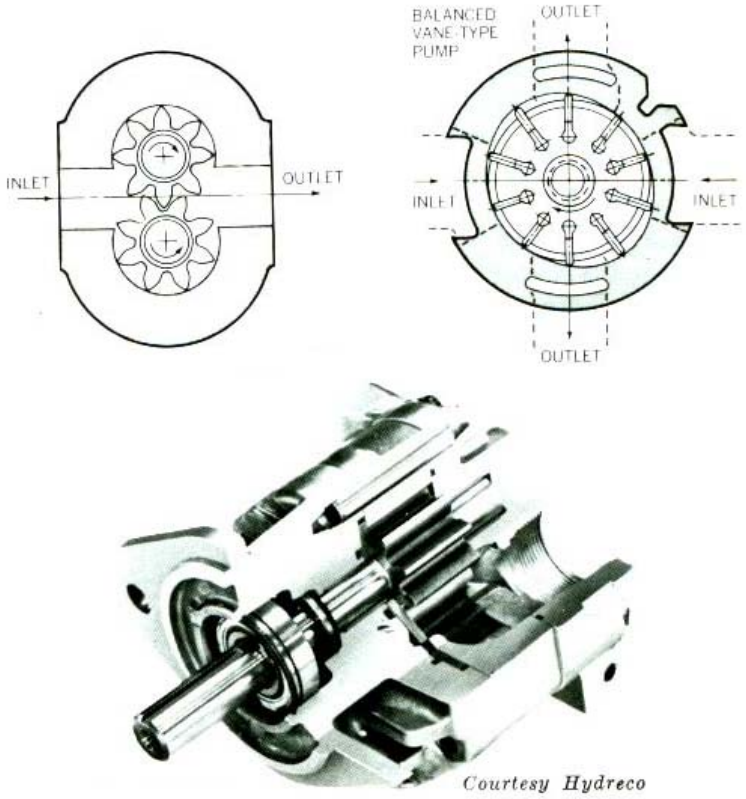

Figure 15. Pumps [11]

Figure 16 shows types of accumulators commonly used in the power input portion of hydraulic systems. Some accumulators employ gaseous medium, and some employ mechanical spring to store the pressure energy in them.

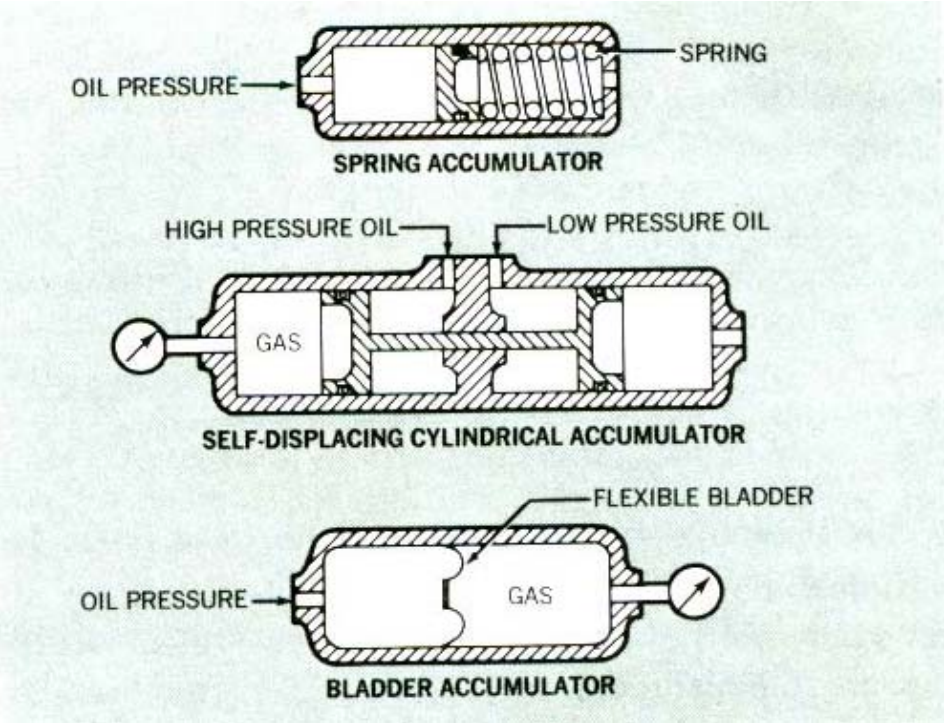

Figure 16. Accumulator [11]

A picture of a control valve is given in figure 17. Control valves control the flow of the pressurized oil from the power input devices. While the job of the power input section of the hydraulic system is to increase the pressure of the operating fluid, the function of the control valves is to regulate the flow of the pressurized fluid to the actuating devices. In general, a six-valve system comprises the control valve portion of the hydraulic system.

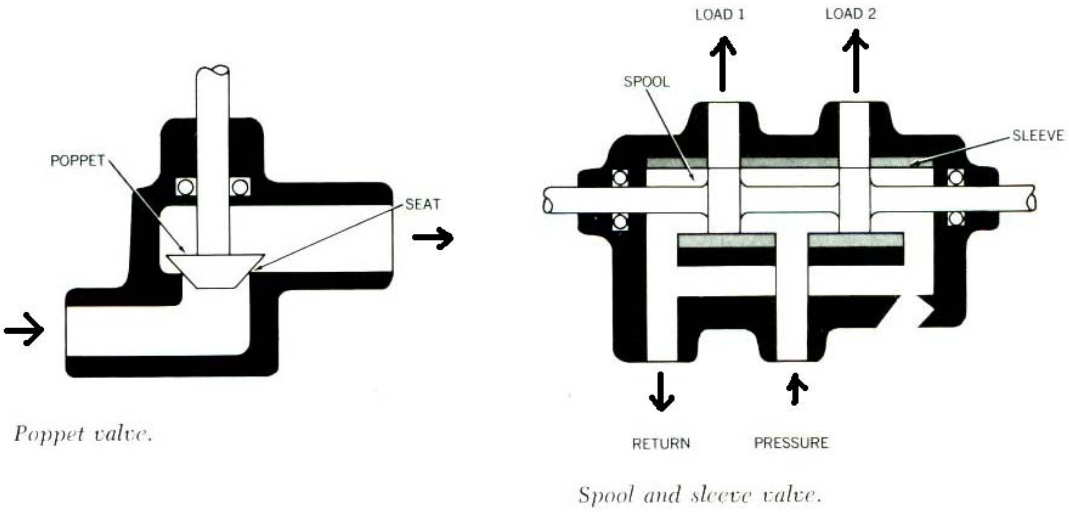

Figure 17. Control Valves [11]

A hydraulic actuator is shown below in figure 18. The actuator converts the energy stored in the pressure of the operating fluid to a mechanical force used to prefrom a task. The control valves determine the amount of force output by the actuator indirectly.

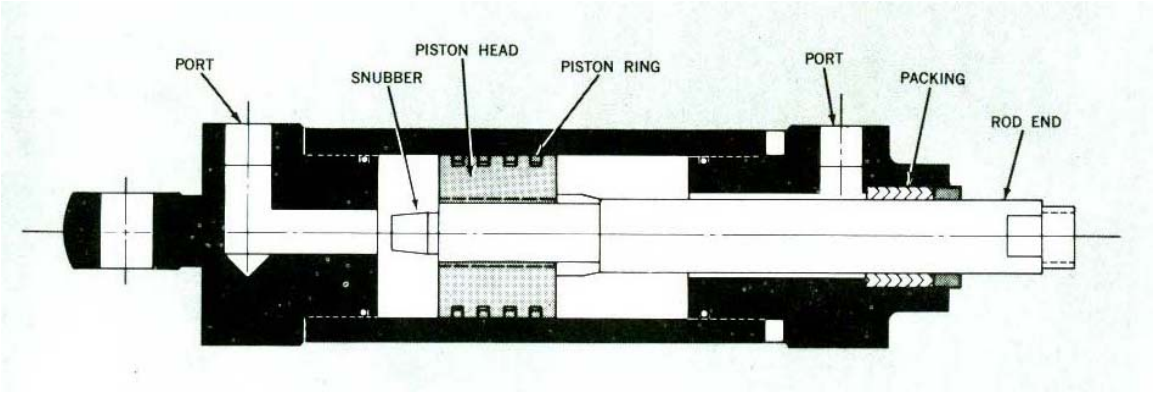

Figure 18. Actuator [11]

Power transmission system of a hydraulic system refers to piping through which the control valves, the power input section, and the power output section communicate. Pipes transmit oil from the pumps or accumulators to control devices. Design of these pipes is based on a cost benefit analysis between energy loss and weight. For example, a large pipe transmits oil flow with less energy losses however it will cost and weigh more.

Modern type of pipes is designed to transmit the oil flow with an average velocity of 15 feet-per-second.

5.1.1 Bolding's Hydraulic System

The hydraulic system designed by Bolding, as shown in figure 19, was comprised of three major assemblies: the hydraulic power supply module, the servo control module, and the model hydraulic actuator system. The operating fluid of the old system was an oil-like fluid. "The hydraulic power supply module is built around and an air-driven hydraulic pump. Air for the pump enters the model from a regulated air supply through a quick-disconnect fitting and a filter." [1] The air was used to pressurize the operating fluid of the system. In Bolding's design, there are many safety features to prevent the catastrophic failure of the system casing in the event of over pressurization. Future groups wishing to design a hydraulic system will benefit from reviewing Bolding's design.

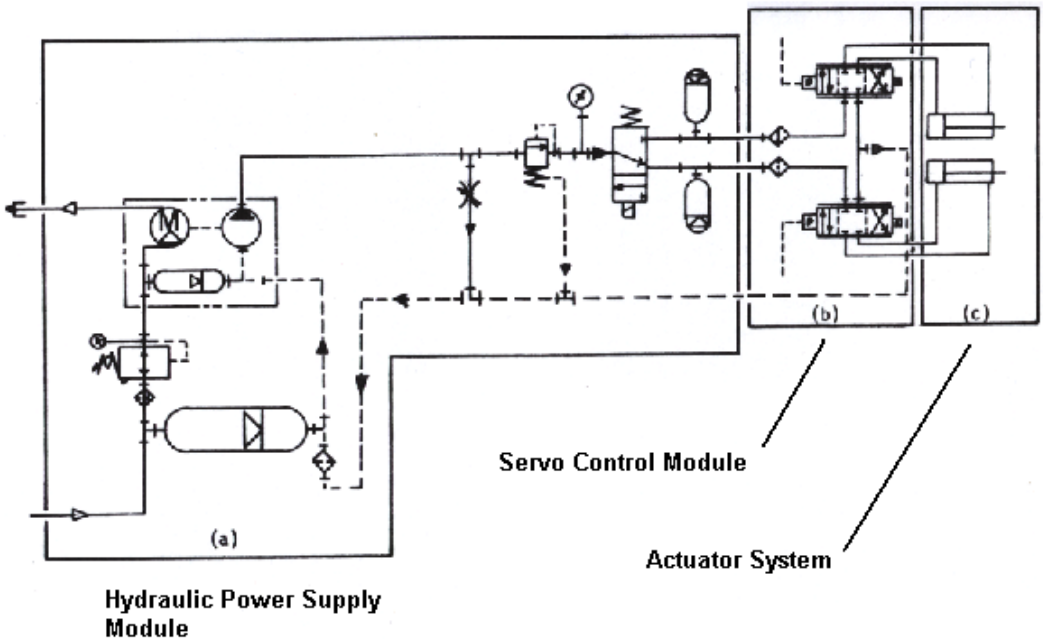

Figure 19 Model Control System [1]

The servo control module, see figure 19 (b), is the *brains* of the hydraulic system. The servo control module regulates the pressure from the power supply to the actuators. Bolding had two actuators connected to the hydraulic system. However, the system could only operate one at a time. The control electronics were used to determine which actuator was to be given energy by the hydraulic system.

5.2 Piezoelectric system

The piezoelectric system is another possible replacement for the outdated hydraulic system. In this section the fundamentals of a piezoelectric power system are discussed. Advantages and disadvantages of the piezoelectric system are also given.

The piezoelectric system is based on piezoelectric effect. When a piezoelectric material is forced to deform in compression or tension, it generates an electrical current. "The effect, discovered by Pierre Curie in 1883, is exhibited by certain crystals, for example, quartz and Rochelle salt, and ceramic materials."[12] To use a piezoelectric material in an actuator, the reverse piezoelectric effect must be utilized. The reverse piezoelectric effect is the opposite phenomenon; when an electrical current is applied onto the opposite sides the piezoelectric material, it elongates. (See figure 20.) When the piezoelectric material is placed inside an actuator, the deformation of the material provides the driving force.

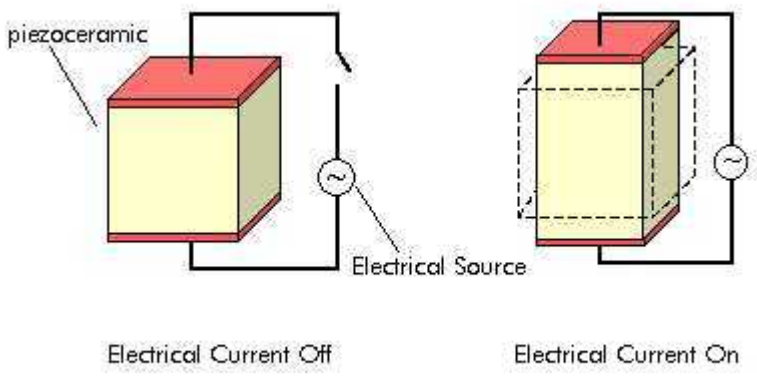

Figure 20. Piezoelectric Material [13=n5]

"A Piezoelectric actuator is an electric type actuator, which converts electrical input energy into an output such as a displacement or generated force." Generally, the piezoelectric actuator has advantages over a hydraulic actuator system. For example, the piezoelectric system has an "extremely rapid response of 0.01 milliseconds, ultra-minute movements of 0.01 microns, and amazing power that exceeds 3 kilograms per square millimeter."[14=n6] On the other hand, a disadvantage of the piezoelectric actuator is that its limited range of movement it can achieve. The limitation is on the order of 0.05 mm [14]. Therefore, its application is also limited for only several fields, and the system is not suitable for AWT's project. Furthermore, the piezoelectric material is brittle, care needs to be taken during use. "High pulling or shear forces must be avoided and this is usually achieved through the design of the actuator and associated mechanical system" [14].

5.3 Magnetic shape memory material

A magnetic shape memory (MSM) material based actuator is the final type of actuator that AWT consider. MSM material is similar to the piezoelectric material. The difference is that the MSM material requires a magnetic field to deform it. As seen in

figure 21 a magnetic field causes the MSM material to deform. The concept of the MSM actuator is the same as the piezoelectric actuator. MSM material is placed inside an actuator casing and a magnetic field is applied. Deformation of the material, while inside the casing, provides the force output of the actuator.

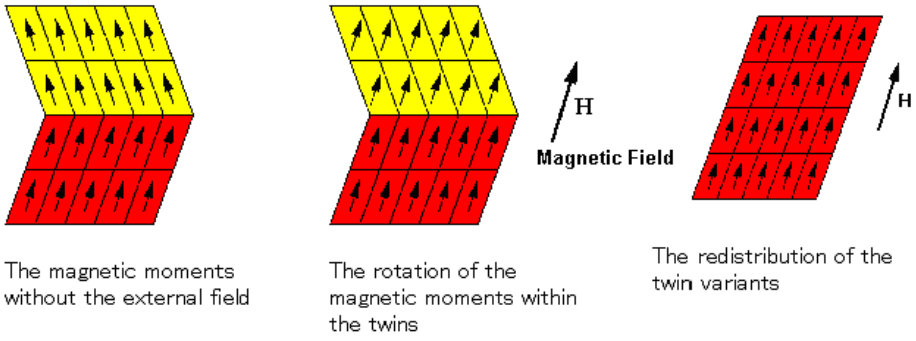

Figure 21. Magnetic Moment [15]

The MSM material may achieve large elastic deformations when an external magnetic field is applied to it. "The largest magnetic field induced deformations have been observed in Ni-Mn-Ga alloys close to the stoichiometric composition Ni_2MnGa, where strains up to 6 % are obtained in the field of 0.6 T."[15]. "In addition to the higher strain, they possess higher energy density, higher coupling factor and they operate at low magnetic field, and complicated shape changes can be produced." [16] Furthermore, large frequency response characteristics of the MSM actuator may be achieved by a rapidly changing magnetic field.

The MSM mechanism has been patented by AdaptaMat Ltd. According to the company, an MSM actuator can achieve a piston stroke of up to 5 mm and forces up to 1.5kN. However, AdaptaMat said that the system would cost over $5000 to meet AWT's requirement of specifications. An AdaptaMat Ltd. MSM based actuator is shown in figure 22.

Figure 22. A Schematic of a Magnetic Shape Memory Material [15]

6.0 Control Electronics

The purpose of the control electronics is to control the wing sweep angle, the pitch of the stabilator, and the motion of the active control surfaces. However, since the implementation of the active control surfaces is still in inchoate stages and the stabilator is missing, only the control electronics as applied to the wing sweep angle is discussed in detail. An overview of the previous analog control system, from 1978, is followed by design and testing of the current analog system. AWT's progress on control electronics will conclude with an overview of the implementation scheme of the digital control system. However, first we will digress and review the necessary background information to fully understand the control electronics.

6.1 Node Voltage Analysis

Before analyzing the amplifying circuits of control electronics, it is necessary to take an aside to refresh our knowledge of node voltage analysis. Node voltage analysis is important to our project in understanding the amplifying circuit analysis in the following sections. Node voltage analysis is based on Kirchhoff's current law, KCL. KCL may be considered the conservation of mass applied to a circuit. KCL states that all the current going into and out of a node must be accounted for. A typical node in a circuit is illustrated below in figure 23

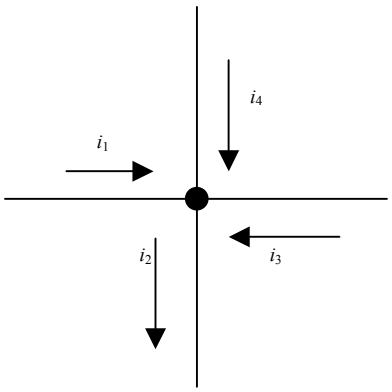

Figure 23 Node in a Circuit

Applying KCL to the node in figure 23 results in the following equation

$$i_1 + i_3 + i_4 = i_2 \qquad [6.1.1]$$

Equation 6.1.1 means that the current going into a node is equal to the current coming out of the node.

Using node voltage analysis, the currents from the KCL equation are written in terms of the voltages at the node. The simple circuit in figure 24 will be used to illustrate node voltage analysis.

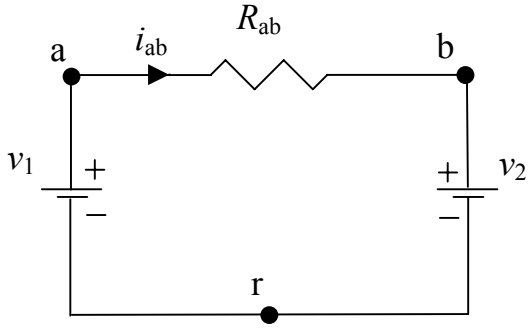

Figure 24. Simple Circuit [17]

Consider the three nodal points, *a*, *b*, and *r*. The voltage across the batteries on the left and right are given by v_1 and v_2, respectively. The reference node is *r*; notice that the

reference node can encompass the entire bottom half of the circuit. The node voltage at node *a* refers to the voltage difference between *a* and *r*:

$$v_a = v_1 \qquad [6.1.2]$$

Likewise, the node voltage at node *b* refers to the voltage difference between *b* and *r*:

$$v_b = v_2 \qquad [6.1.3]$$

Typically the reference node, *r*, is grounded, i.e. voltage equals zero. Therefore, the node voltage at node *a* and *b* would be the true voltage and not just the voltage change from the reference.

As mentioned before, the purpose of the node voltage technique is to describe the currents in terms of the node voltages. In figure 24the current from *a* to *b*, i_{ab}, is the voltage at *a* minus the voltage at *b* divided by the resistance between *a* and *b*

$$i_{ab} = \frac{v_a - v_b}{R_{ab}} = \frac{v_1 - v_2}{R_{ab}} \qquad [6.1.4]$$

The statement above concerning the current, i_{ab}, is the main purpose of the node voltage technique; it serves as a mnemonic device to express the current. However, the statement only applies to nodes with resistors between them. The node voltage technique is favorable in analyzing electronic circuits, such as those containing op amps, because many of the components are always grounded. Thus each component can have the same reference node.

6.2 Operational Amplifier Analysis

An operational amplifier, or op amp for short, is the most important component in an analog control system. Op amps may be used to do calculations such as integration, summation, and even logarithmic calculations. For the purposes of this project, the op

amp is the 'brains' of the control system. The op amp compares the reference value with the actual value and outputs the necessary value to control the process. This project relies specifically on two specific op amp techniques: the summing amplifier and the inverting amplifier.

There exists a possible source of confusion when referring to an amplifying circuit and an op amp. An op amp is a component of a summing amplifier or an inverting amplifier. Consequently, referring the gain of the op amp differs from the gain of the entire amplifying circuit; the same applies to the current, voltage, etc.

6.3 Inverting Amplifier

The schematic of an inverting amplifier is shown below in figure 25The inverting amplifier circuit is composed of an op amp; two resistors, R_i, and R_F; and an input voltage signal, v_1. Analysis of the inverting amplifier is based on the assumptions that the op amp is operating in its linear amplifying region and that the gain of the op amp is very high [17]. The assumption that the op amp is operating in its 'linear amplifying region' is expresses by the input-output characteristics as shown in figure 26

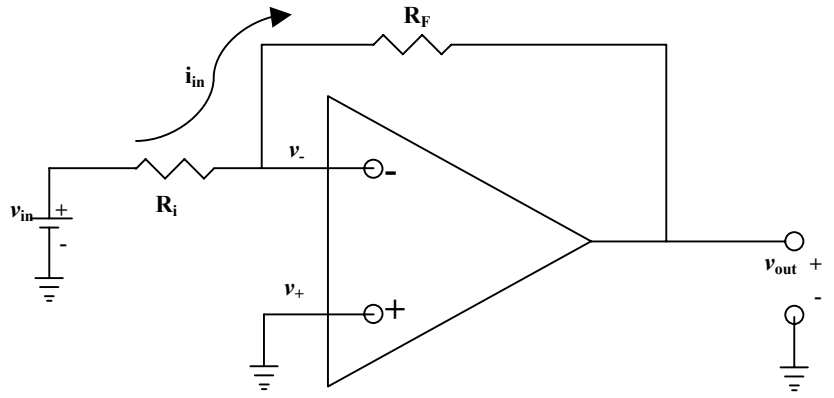

Figure 25. Inverting Amplifier

Figure 26 shows that the op amp is governed by the following equation

$$v_+ - v_- = \frac{v_{out}}{A} \qquad [6.3.1]$$

Equation 6.3.1 states that the output voltage, v_{out}, of the op amp is equal to the difference between the voltage at the input terminals, v_+ - v_-, times some gain, A. The assumption that the gain of the amplifier is very high leads to the following equation:

$$v_+ - v_- \approx 0 \Rightarrow v_+ \approx v_- \qquad [6.3.2]$$

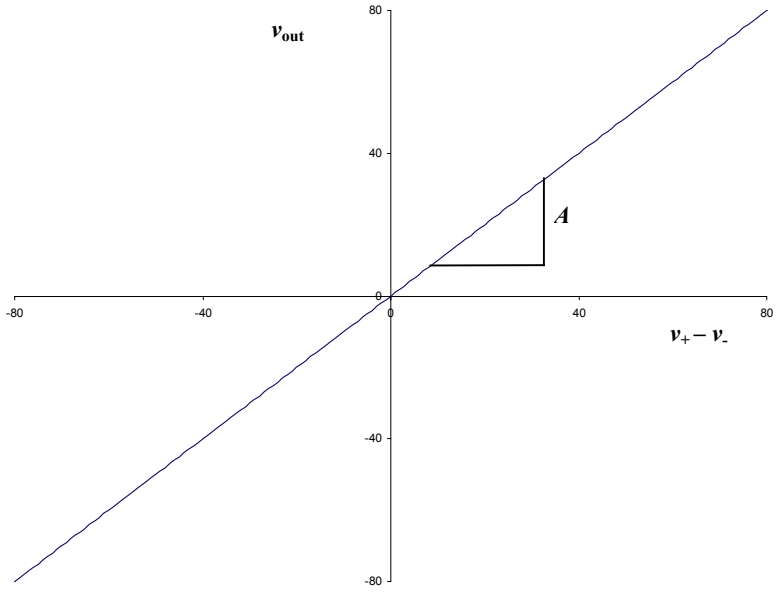

Figure 26. Output Characteristics of Op Amp

For instance, if $v_{out} < 15$ volt and $A = 10^6$, then $v_+ - v_- < 15/10^6 = 15$ μV. Therefore, the voltages at the input terminals, v_+ and v_-, will be equal within 15 μV or less. Furthermore, for the schematic in figure 25, the positive input terminal of the op amp is grounded; consequently, $v_+ = 0$ and $v_- \approx 0$. Thus, the current resulting from v_{in} may be written using the node voltage analysis technique from section 6.1

$$i_{in} = \frac{v_{in} - v_-}{R_i} \approx \frac{v_{in}}{R_i} \qquad [6.3.3]$$

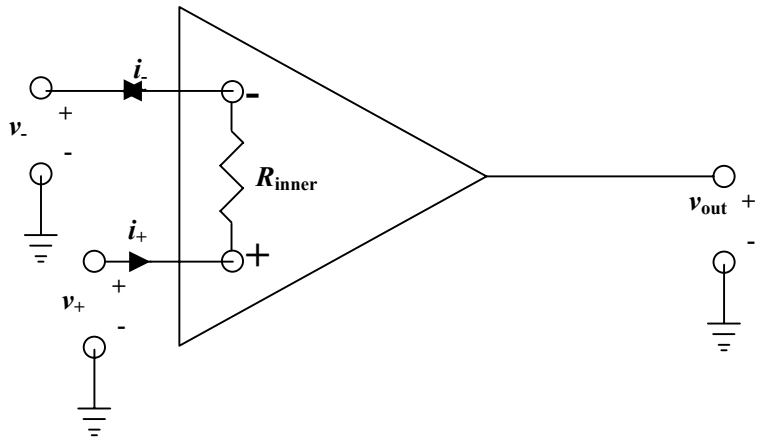

Figure 27. Inner Resistance of Op Amp

The inner resistance, R_{inner}, between the input terminals of the op amp is illustrated in figure 27. Typically, the resistance between the input terminals has a large value of resistance; this results in negligible current into the positive and negative terminals of the op amp

$$\left|i_{+}\right| = \left|i_{-}\right| = \frac{\left|v_{+} - v_{-}\right|}{R_{inner}} \approx 0 \qquad [6.3.4]$$

Negligible current into the negative input terminal of the op amp in figure 25 implies that the current that flows through R_{i} is the same current that flows through R_{F}. Therefore, using i_{in}, the output voltage of the inverting amplifier circuit may be calculated

$$v_{-} - v_{out} = i_{in} R_F \Rightarrow v_{out} = -\frac{v_{in}}{R_i} \cdot R_F \qquad [6.3.5]$$

Rearranging equation 6.3.5, the voltage gain of the entire inverting amplifier circuit may be expressed as follows

$$\frac{v_{out}}{v_{in}} = -\frac{R_F}{R_i} \qquad [6.3.6]$$

Equation 6.3.6 shows that an inverting amplifier may be used to change the polarity of an incoming voltage signal; this property of the inverting amplifier's gain is useful in conjunction with a summing amplifier.

6.4 Summing Amplifier

A summing amplifier is a modification of an inverting amplifier as shown in figure 28. Notice that the summing amplifier is the inverting amplifier, from figure 25, plus an additional input voltage signal. The summing amplifier circuit consists of three types of components: three resistors, R_1, R_2, and R_F; two input voltage signals, v_1 and v_2; and an op amp.

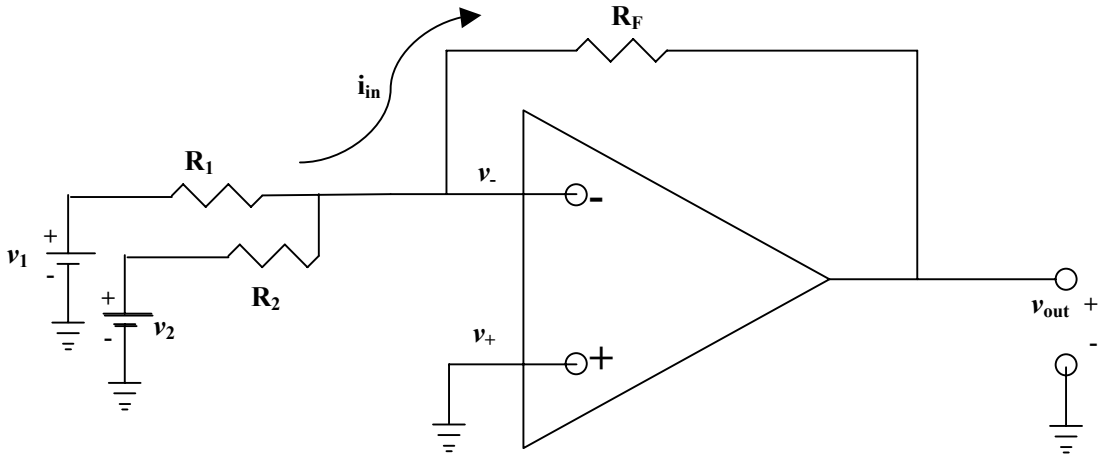

Figure 28. Summing Amplifier

Using the same assumptions from the inverting amplifier section, the op amp gain is large and is operating in its linear range; analysis of the summing amplifier is similar to the inverting amplifier. The difference between them is the calculation of the current coming from the two voltage inputs. The input current from the voltage source, i_{in}, is calculated using the node voltage technique

$$i_{in} = \frac{v_1 - v_-}{R_i} + \frac{v_2 - v_-}{R_2} \approx \frac{v_1}{R_i} + \frac{v_2}{R_2} \qquad [6.4.1]$$

Recall from section 6.3, since the positive input terminal of op amp is grounded, $v_+ = 0$; the input voltage of the negative terminal of the op amp is approximately zero, $v_- \approx 0$. The output voltage of the summing amplifier, v_{out}, draws the input current, i_{in}, through R_F; the output voltage may be determined as follows

$$v_- - v_{out} = i_{in} R_F \Rightarrow v_{out} = -\left(\frac{v_1}{R_i} + \frac{v_2}{R_2}\right) \cdot R_F = -\left(\frac{R_F}{R_i} \cdot v_1 + \frac{R_F}{R_2} \cdot v_2\right) \quad [6.4.2]$$

Equation 6.4.2 shows the output voltage as the negative of the weighted sum of the input voltages. The negative polarity of the output voltage of the summing amplifier is a problem that may be addressed by adding an inverting amplifier. An example is shown in figure 29.

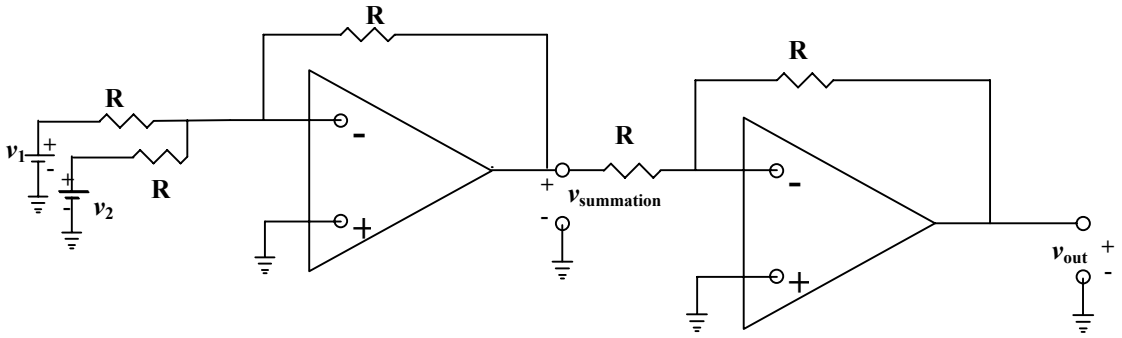

Figure 29. Summing Amplifier Combined with Inverting Amplifier.

For simplicity, the resistance values throughout the schematic in figure 29 are all equal. The output voltage of the summing amplifier is calculated from equation 6.4.2

$$v_{summation} = -\left(\frac{R_F}{R_i} \cdot v_1 + \frac{R_F}{R_2} \cdot v_2\right) = -(v_1 + v_2) \quad [6.4.3]$$

The output voltage of the summing amplifier is now the input voltage source of the inverting amplifier. The final output voltage of the summing amplifier/inverting amplifier system is determined by substituting the output voltage of the summing amplifier for the input voltage of the inverting amplifier in equation 6.3.6

$$\frac{v_{out}}{v_{in}} = -\frac{R_F}{R_i} = -1 \Rightarrow v_{out} = -v_{in} = -\left(-\left(v_1 + v_2\right)\right) = v_1 + v_2 \qquad [6.4.4]$$

6.5 Block Diagrams of Closed Loop Feedback Systems

A review of the block diagram representation of a control system is provided in this section. A standard closed loop feedback system is presented in block diagram form as shown in figure 30. The purpose of the control system is to control the output variable, Y. Ideally, the output variable is supposed to mirror the input variable, R. Each block in the diagram represents a major component of the control system. The chain of occurrences in a feedback system begins with the input. The input is the reference value that output should equal. The actual value of the output is obtained by the sensor and compared to the input. The difference between the input value and the output value is the error. The error is input into the controller, G_C. The purpose of the controller is to reduce the error. The signal from the controller is then input to the actuator, G_A. An actuator is the device that converts the signal from the controller to a mechanical force. The force applied by the actuator changes the output according to some governing equations of motion inherent to the process dynamics block, G_p. The output, Y, is again measured by the sensor and compared to the input to determine the error. Hence the name closed loop feedback system.

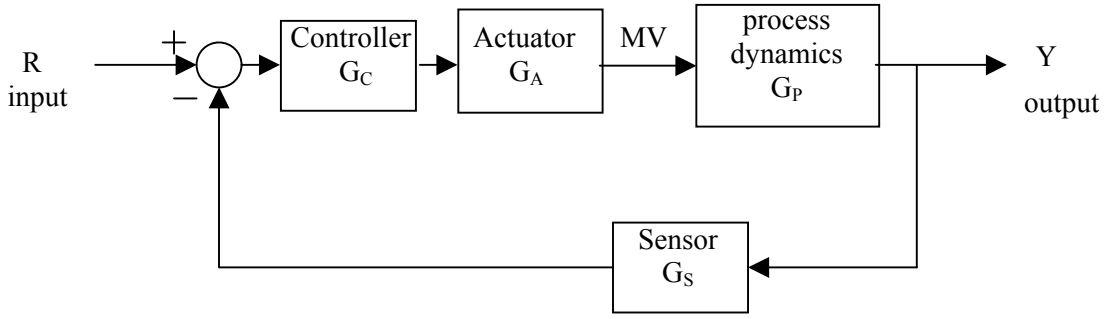

Figure 30. Basic Block Diagram

In the block diagram representation, each block represents a mathematical model of the equations of motion governing a particular part of the system. Typically, the equations of motion are derived in the form of a differential equation expressed as a function of time. However, in the block diagram representation, the equations of motion are transformed from the time domain to the s-domain with a LaPlace transform. The purpose of the transformation is that a differential equation in the time-domain may be reduced to a polynomial in the s-domain. For instance, consider the equations of motion governing the *process dynamics* block. Assume that the relationship between the signal from the actuator, MV(s), and the output of the system, Y(s), may be expressed by the differential equation as follows

$$A \cdot \frac{d^2}{dt^2}\big(y(t)\big) + B \cdot \frac{d}{dt}\big(y(t)\big) + C \cdot \big(y(t)\big) = Q \cdot \frac{d}{dt}\big(mv(t)\big) + R \cdot \big(mv(t)\big) \qquad [6.5.1]$$

A, B, C, Q, and R are arbitrary coefficients. By convention, a variable expressed in lower case is representative of the time domain; a variable expressed in upper case symbolizes the s-domain. The LaPlace transformation of equation 6.5.1 is shown in the following steps. A table of LaPlace transformations is given in Appendix B.

$$\mathbf{L}\left\{ A \cdot \frac{d^2}{dt^2}\big(y(t)\big) + B \cdot \frac{d}{dt}\big(y(t)\big) + C \cdot \big(y(t)\big) = Q \cdot \frac{d}{dt}\big(mv(t)\big) + R \cdot \big(mv(t)\big) \right\} \qquad [6.5.2]$$

$$\Rightarrow A \cdot \left[s^2 \cdot Y(s) - s \cdot y(0) - \dot{y}(0) \right] + B \cdot \big[s \cdot Y(s) - y(0) \big] + C \cdot Y(s) = Q \cdot \big[s \cdot MV(s) - mv(0) \big] + R \cdot MV(s)$$

The transfer function may be considered the ratio of the output to the input of the block in a block diagram. Assuming all initial conditions are zero, the transfer function is given by the following equation

$$G_p = \frac{Y(s)}{MV(s)} = \frac{Qs + R}{As^2 + B + C} \qquad [6.5.3]$$

A general representation of a transfer function is presented below

$$G = \frac{p(s)}{q(s)} \qquad [6.5.4]$$

In general the transfer function, *G*, is a quotient of two polynomial functions, *p(s)* and *q(s)*. As mentioned before, the LaPlace transform allows the differential equation in the time-domain to be represented as a polynomial in the s-domain. The polynomial expression of the differential equation is written in the blocks of the block diagram. The output of the block is always the transfer function of the block times whatever is input to the block

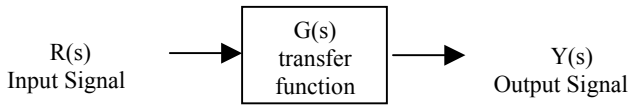

$$Y(s) = G(s) \cdot R(s)$$

6.6 Bolding's Analog System

This section is provided as a review of the original analog circuitry used with the wing-stabilator model. The previous analog control system is shown in figure 31. In this context, analog means that information is encoded into an electrical signal that it is proportional to the quantity being represented [17]. For example, in this particular project, measurements of the wing sweep angle or the pitch of the stabilator are taken with Direct Current Differential Transformers (DCDT). A DCDT is a transducer calibrated such that a measured wing sweep angle or stabilator pitch angle outputs a corresponding voltage.

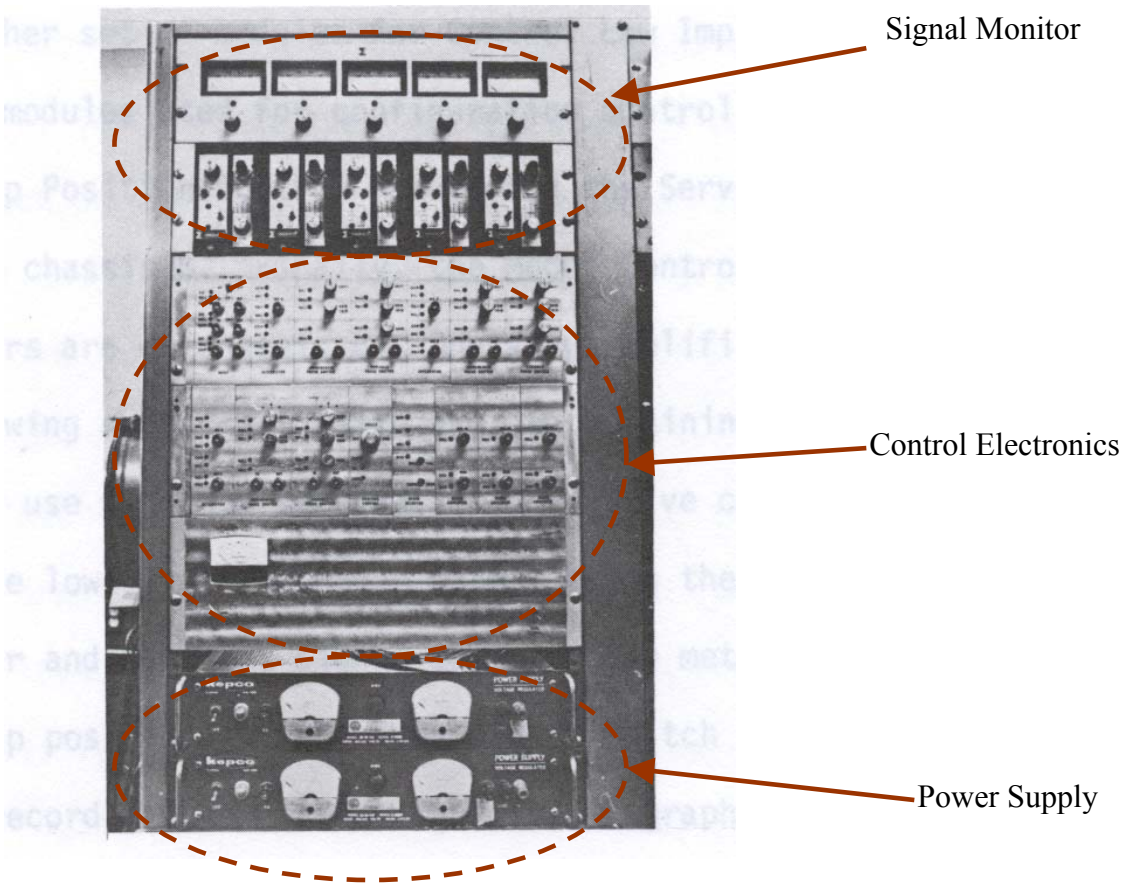

Figure 31. Analog Control Electronics System [1]

The top panel of the analog system, shown in figure 31 above, is the signal monitor; it is used in monitoring the incoming accelerometer signals. The bottom element is the power supply. The power supply's main function was to provide energy to move the stabilator; however, when a change in the wing sweep was desired, power was diverted from the stabilator to the wing. The remaining three elements are the control electronics. The control electronics are composed entirely of electronics modules. The advantage of the modular construction is that it allows the quick replacement of defective circuits and testing on a modular basis. [1] The function of the control electronics belongs

to two subsystems: The Configuration Control System and the Control Law Implementation System.

6.6.1 Configuration Control System

The function of the configuration control system is to control the wing sweep position. The entirety of the configuration control system is composed of three major electronic components: the position control module, the Servo-selector, and the Servoamplifier. The components are shown in figure 32.

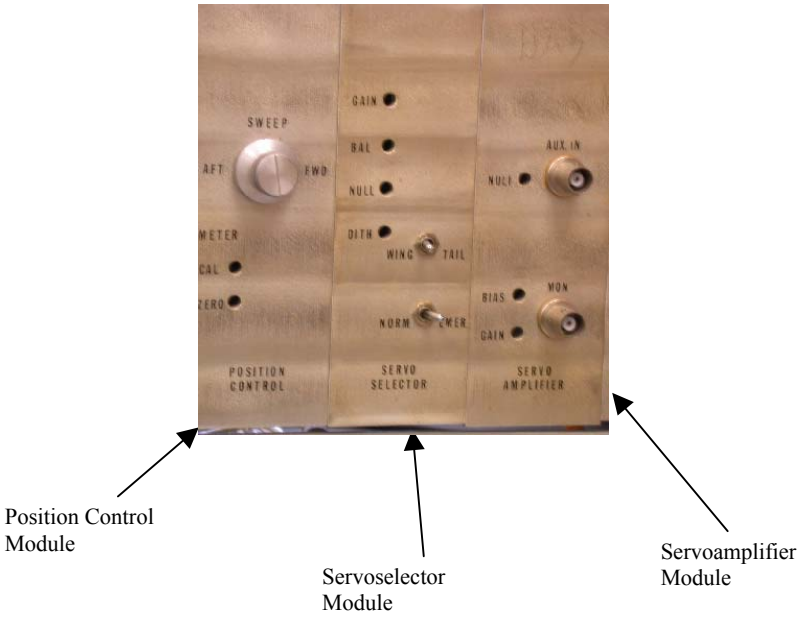

Figure 32. Configuration Control System

Figure 33 shows a schematic of the configuration control system.

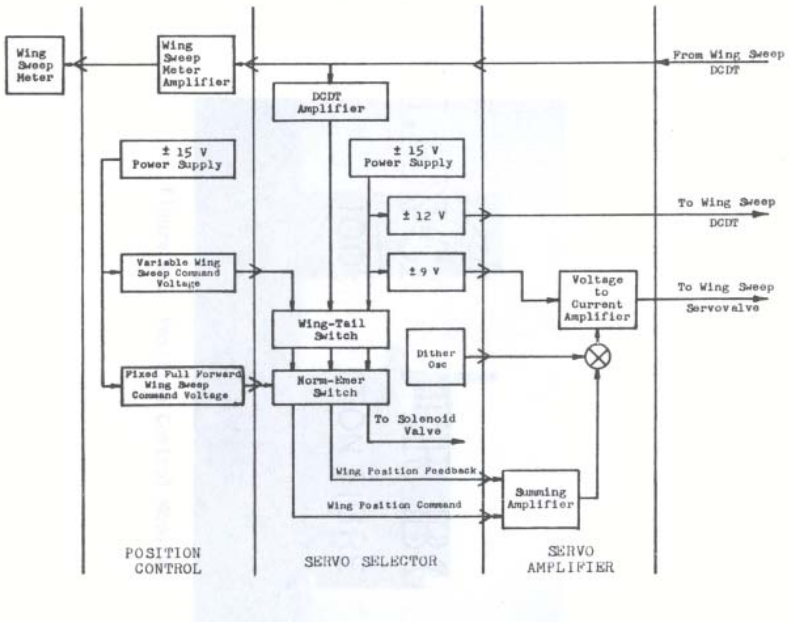

Figure 33. Schematic of Configuration Control System

Notice the position control section in figure 33 above. The purpose of the position control module is two fold:

- Amplify the signal from the wing sweep position sensor to a powerful enough signal for the wing sweep meter. The wing sweep meter is calibrated to physically display the current angle of the wing sweep.
- Provide a wing sweep command in the form of a variable voltage.

The function of the wing sweep meter amplifier is trivial but necessary. The signal coming from the wing sweep sensor is too weak to drive the wing sweep meter; the amplifier adds energy to the signal to drive the wing sweep meter. The wing sweep meter is shown below in figure 34.

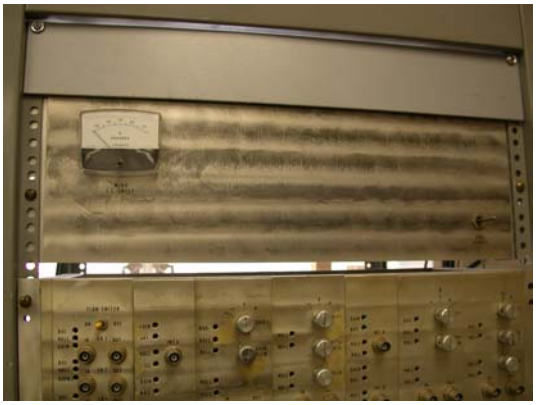

Figure 34. Wing Sweep Meter

A power supply in conjunction with a series of resistors, as shown in figure 35, provides a variable voltage to set off a series of reactions within the circuitry to drive the wing sweep position. The output voltage of the circuit in figure 35 is calibrated to represent a particular wing sweep angle. For example, an output voltage of 5 volts might represent the fully swept forward wing on the display of the wing sweep meter, while an output voltage of -5 volts would represent a fully aft wing on the wing sweep meter display.

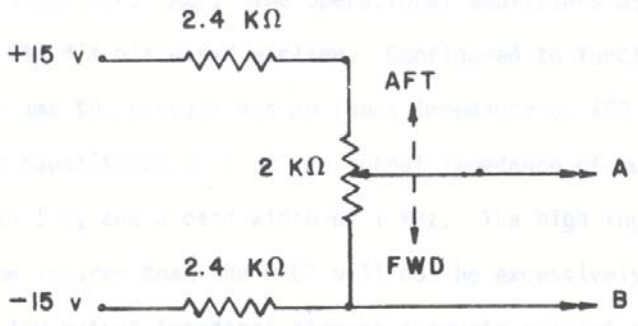

Figure 35. Wing Sweep Control

Turning the knob on the position control module varies the voltage output which initiates a chain of occurrences that lead to actually moving the wing; the next step in the chain of occurrences begins with the servo-selector module.

In the servo-selector module, the variable voltage from the position control module along with the feedback from the position sensor from the wing is input into two wing-stabilator/norm-emergency switches. The switches, which are manually operated, are shown on figure 36.

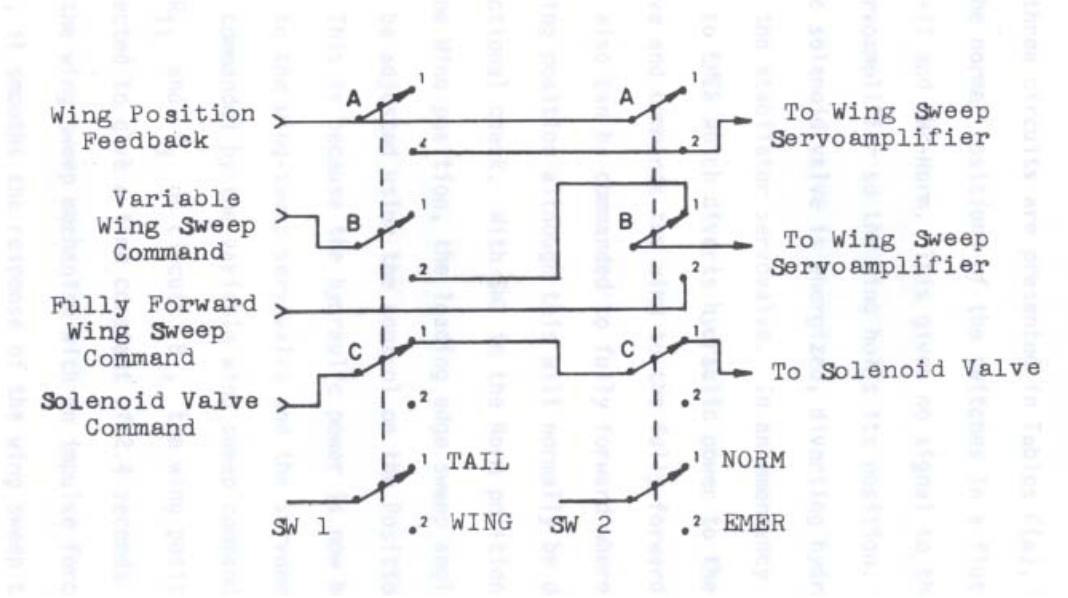

Figure 36. Wing-Stabilator/Norm-Emergency Switches [1]

The purpose of the switches is to allow the operator to determine the "state" of operation. For example, the wing-stabilator switch basically determines whether power is given to the wing or the stabilator, but the norm-emergency switch is primarily for the wing. In "normal" mode, depending on the position of the wing-stabilator switch, the wing sweep can be controlled with the wing sweep control knob on the position control module or the stabilator can be controlled with the control laws implemented in the servo-amplifier module, explained in the next section. However, when in "emergency" mode, the wing is swept fully forward so as to stave off the onset of flutter and preserve the model.

In addition to the wing-stabilator/norm-emergency switches, the servo-selector module is home for another power supply for the Wing Sweep DCDT, a solenoid valve,

and a voltage to current amplifier in the servoamplifier module. The solenoid value is the medium by which power is given to either the wing or the stabilator. The wing-stabilator/norm-emergency switches control whether or not power is given to the solenoid valve. The solenoid valve in turn determines whether hydraulic power is given to the wing or the stabilator. A DCDT amplifier also resides in the servo-selector module. Similar to the wing sweep meter amplifier in the position control module, the DCDT amplifier buttresses the feedback signal from the DCDT position sensor on the wing to a signal usable by the wing-stabilator/norm-emergency circuitry. The next step in the configuration control system is the servoamplifier module

The servoamplifier module is similar to the summing amplifier/inverting amplifier schematic shown in figure 29. The additional diodes, capacitors, and transistors serve as protections devices in the circuit. A schematic of the servoamplifier is shown in figure 37 below.

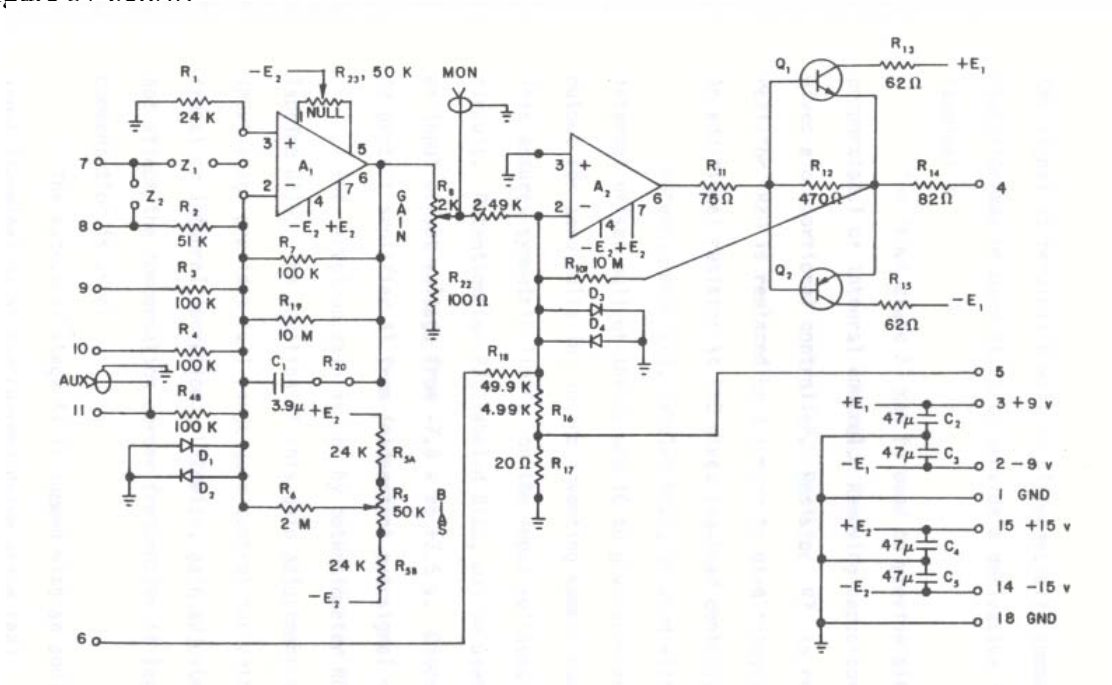

Figure 37. Schematic of Servoamplifier [1]

Details involved in understanding the circuitry of the servoamplifier module are not necessary because AWT found no use for the servoamplifier electronics. For simplicity, the servoamplifier module of the Configuration Control System is considered a "black box" proportional controller. A basic closed loop feedback block diagram control system is presented in figure 38.

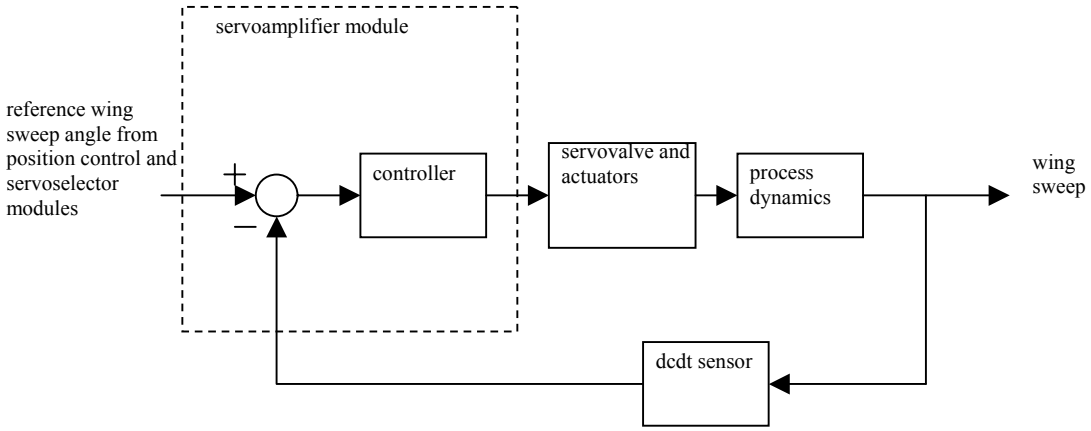

Figure 38. Block Diagram of Configuration Control System [1]

The servoamplifier module is highlighted in figure 38. Wing sweep reference angle information and the actual wing sweep position information are both input to the Servoamplifier module. The servoamplifier module is designed to interpret magnitude of the incoming voltage as representative of the actual wing sweep angle. The error, the difference between the desired reference value and the actual value, is then computed and input to the controller section of the Servoamplifier module. The controller then outputs the necessary controls actions, in the form of voltage, to the servo valve and actuators to move the wing. The means by which the error is computed and the controller performs the necessary control action is governed by the transfer functions of the "black box" circuitry of the Servoamplifier module.

6.6.2 Control Law Implementation System

The purpose of the Control Law Implementation System is to process the data from the acceleration sensors on the stabilator and wing and perform the necessary control actions to vary the pitch of the stabilator in order to suppress flutter. Control laws are used to determine the control actions necessary to suppress flutter given position and acceleration data from the sensors. A control law is a theoretical model of the process. For example, if the aerodynamic forces change the pitch of the stabilator, the control law attempts to predict the motion of the wing-stabilator system. Using the prediction of motion, control actions can be taken to suppress undesired motions of the system.

Implementation of the Control Law System is the most academically challenging aspect of this project. Bolding's work on control law implementation using analog control systems is very difficult to understand. Before trying to follow the control law implementation scheme of Bolding, AWT recommends that any future groups begin by learning some of the basics in advanced control law theory.

6.7 Current Analog Control System

The analog control system presently in use is shown below in figures 38 and 40. The Educational Servo model es151, shown in figure 39, is a pre-fabricated circuit made by Feedback Co. An electrical circuit diagram of the entire circuit is given in Appendix A.

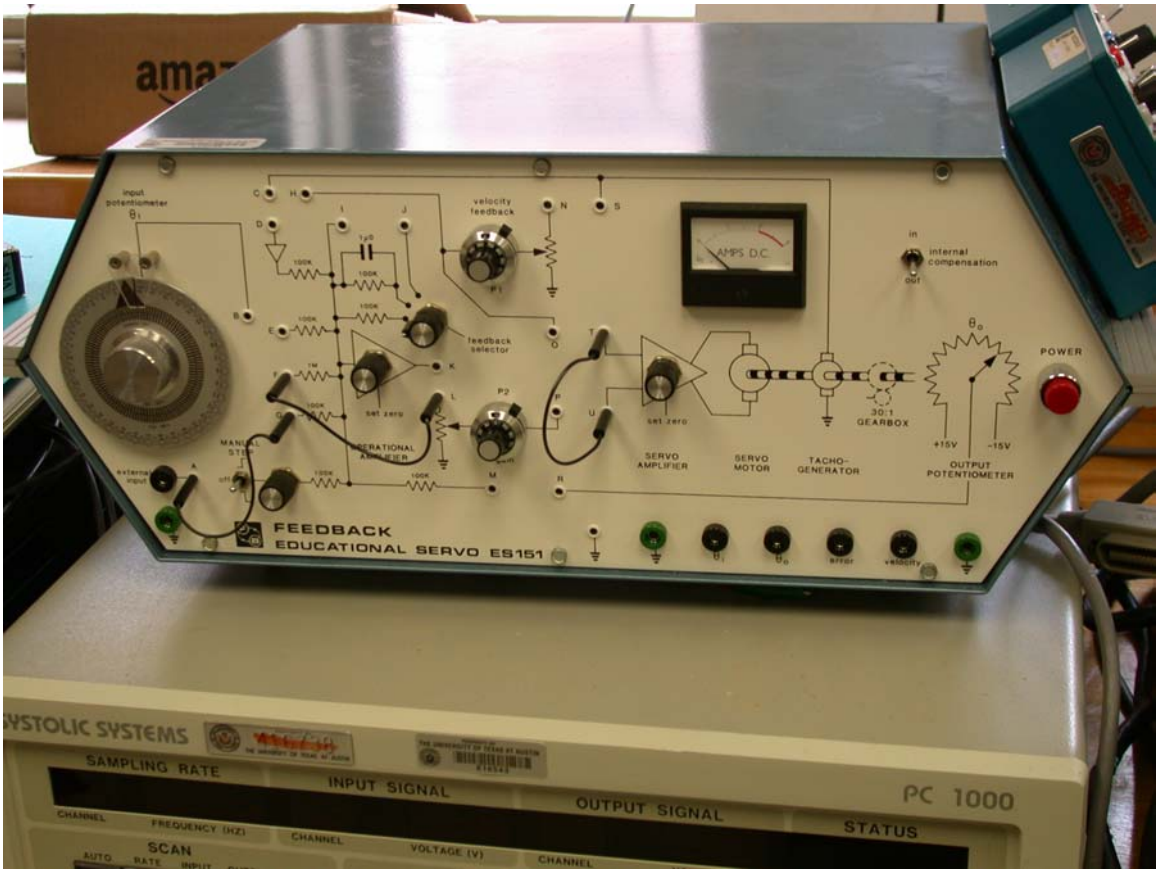

Figure 39. Educational Servo Model ES 151a

The Educational Servo model ES 151b, shown in figure 40, is the motor designed for use in conjunction with model ES 151. The circuitry of the Educational Servo may be made to control either the position or rotational speed of the model.

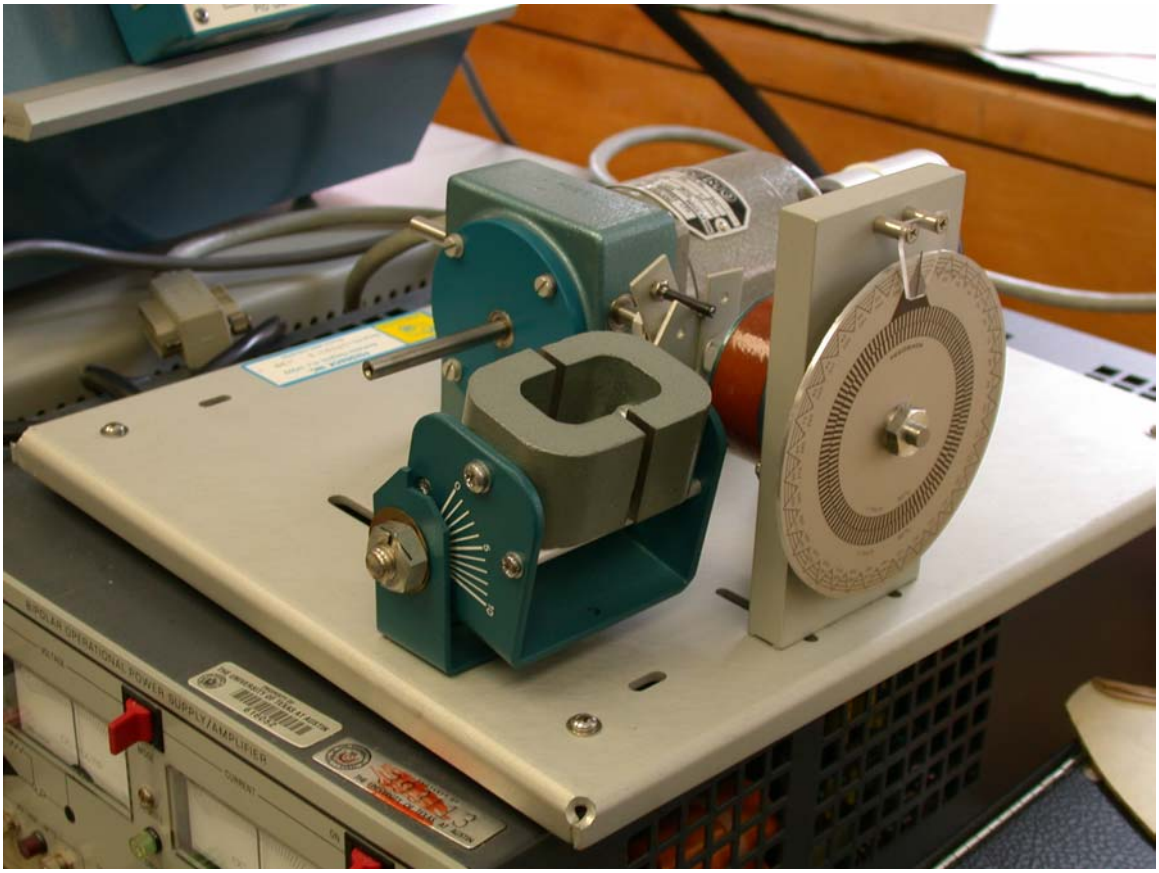

Figure 40. Educational Servo Model ES 151a

The Educational Servo System, shown in figures 39 and 40, is presented in terms of a block diagram in figure 41.

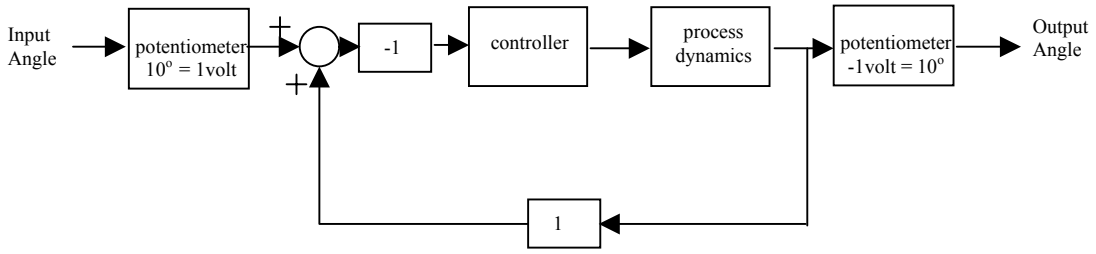

Figure 41. Block Diagram of ES 151 System

A walkthrough of the diagram begins with the input angle. The circular dial on the left of figure 39 is used to set a specific input angle. A potentiometer is calibrated to

output a particular voltage for a given angle. Notice that the block diagram in figure 41 is a positive feedback loop instead of a negative feedback loop from figure Z. The positive feedback and the block with the "-1" are used to represent the actions of the summing amplifier in the circuit. The summing amplifier outputs the negative of the sum of the input voltage and the output voltage. The transfer functions of the summing amplifier are derived in section 6.4. The output of the summing amplifier is considered the error. The error is the difference between the input angle and the displayed angle on the ES 151b. Notice that the error is still the difference of the input and the output voltage. As mentioned before the summing amplifier outputs the negative of the sum of two voltages. Feeding back the negative of the sum implicitly produces a negative feedback.

The error is then input to the controller. The job of the controller is to output a voltage signal that reduces the error. The implementation of four major types of analog process controllers using analog circuitry is discussed in Appendix D. The four types of controllers discussed are a proportional, proportional-derivative, proportional-integrating, and a proportional-integrating-derivative. The name of the controller refers to the form of its transfer function in the s-plane. Furthermore, in Appendix D, the differential equation of the analog circuitry has been derived and converted to the s-plane to show that the circuit provides the desired transfer function. The goal of Appendix D is to show the multiple types of transfer functions available for G_c in figure 41.

The process dynamic block is a model of everything that occurs beginning with an input signal from the controller to the voltage signal fed back to the summing amplifier. In general, obtaining a mathematical model of the process dynamics is the most time consuming and costly component a controls project. Fortunately, one of the

advisors to AWT, Dr. Senent, hinted that the model of the Educational Servo from the power amplifying stages to the motor out was a second order system. The process of finding the process of the model and validating the model are discussed in sections 6.8 and 6.9.

6.8 Modeling the Process Dynamics

Dr. Senent suspected that the process dynamics block in figure 41 would be of the form as follows.

$$G_p(s) = \frac{K}{s \cdot (\tau s + 1)} \qquad [6.8.1]$$

To determine if the suspicion is correct, the response of the motor to a known input signal must be observed; this lead to AWT's first hands-on experiment. The first step in conducting the experiment was to isolate the transfer function block of the process dynamics as shown in figure 42.

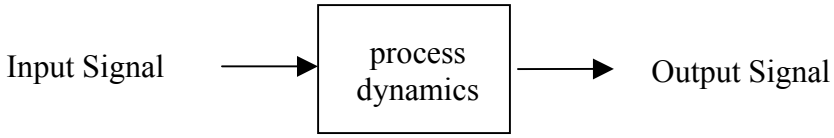

Figure 42. Isolating the Process Dynamics Block

The idea was to input a known voltage signal and observe the form of the output. If the output response is similar to the graph in figure 43, then the transfer function of the process dynamics is of the form in equation 6.8.1.

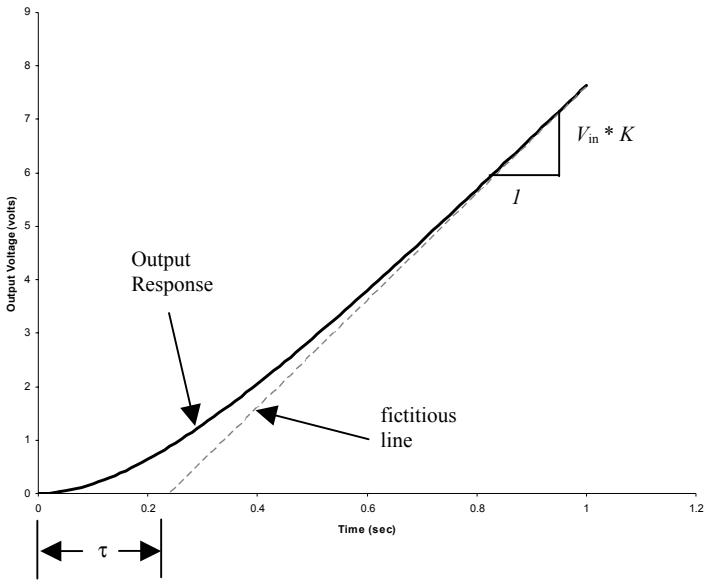

Figure 43. Response of Second Order System

Isolating the process dynamics block on the Educational servo is presented in figure 44.

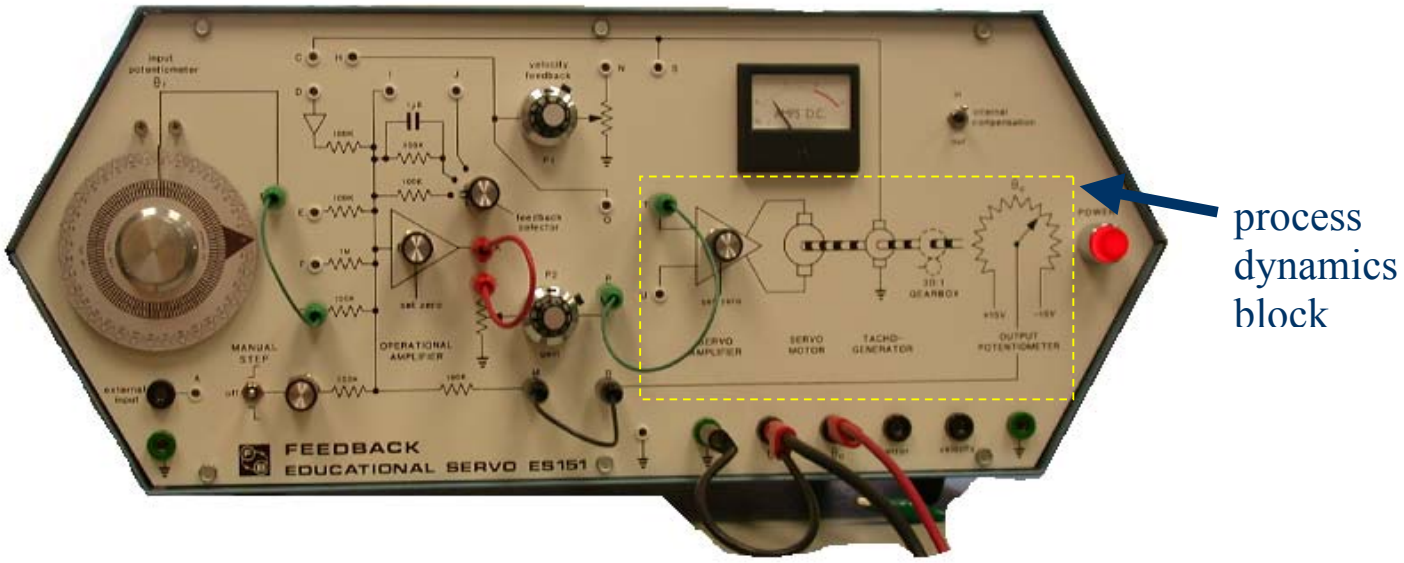

Figure 44. Process Dynamics Block on Educational Servo

On the face of the Educational Servo system exists female plugs labeled ‘A’ through ‘R’. The process dynamics of the position control was isolated by inputting a known voltage into the female plug labeled ‘T’ and measuring the response at the plug labeled ‘R’. A

digital oscilloscope was needed to take the measurement of the response of the output. To the delight of AWT, the output response of the process dynamics was observed to be similar to the graph in figure 43. The response is shown in figure 45. This meant that the time constant, τ, and the gain of the process dynamics block, K, could be measured off of the graph and then a mathematical model of the process dynamics may be determined.

Figure 45. Picture of response on the oscilloscope.

Before data was taken, an analysis of how to get the coefficients off of the display of the oscilloscope was conducted. According to the table of Laplace Transforms in Appendix B an input step voltage of V_{in} would be of the following form in the s-domain

$$R(s) = \frac{V_{in}}{s} \qquad [6.8.2]$$

Therefore the output of the process dynamics block of the form in equation 6.8.1 would be as follows

$$Y(s) = G_p(s) \cdot R(s) = \frac{K}{s \cdot (\tau s + 1)} \cdot \frac{V_{in}}{s} = \frac{a}{s^2} + \frac{b}{s} + \frac{c}{s + 1/\tau} \qquad [6.8.3]$$

The technique of partial fraction expansion is need to determine the coefficients, *a*, *b*, and *c*. A review of partial fractions is given in Haykin [18]. The coefficients *a*, *b*, and *c* were

found to be $V_{in} \cdot K$, $-V_{in} \cdot K \cdot \tau$, and $V_{in} \cdot K \cdot \tau$, respectively. Therefore, the output of the process dynamics block is as follows

$$Y(s) = \frac{V_{in} \cdot K}{s^2} - \frac{V_{in} \cdot K \cdot \tau}{s} + \frac{V_{in} \cdot K \cdot \tau}{s + 1/\tau} \qquad [6.8.4]$$

The inverse Laplace transform was then used to convert the output of the process to the time domain. The inverse Laplace transform was taken from tables in Appendix B. The result was simplified as follows

$$y(t) = V_{in} \cdot K \cdot t - V_{in} \cdot K \cdot \tau + V_{in} \cdot K \cdot \tau \cdot e^{\frac{-t}{\tau}} = V_{in} \cdot K\left[t + \tau\left(e^{\frac{-t}{\tau}} - 1\right)\right] \qquad [6.8.5]$$

Equation 6.8.5 may be manipulated to determine the coefficients $V_{in} \cdot K$ and τ. Take the limit of y(t) as *t* goes to infinity

$$\lim_{t \to \infty} y(t) = V_{in} \cdot K[t - \tau] \qquad [6.8.6]$$

With the equation for the output written in this form, we can draw a fictitious line as seen in figure 43. The slope of the line is $V_{in} \cdot K$. The slope, *m*, can be read off of a digital oscilloscope and with the value of the input voltage, the gain of the process dynamics, *K*, can be determined as follows

$$K = \frac{m}{V_{in}} \qquad [6.8.7]$$

The time constant, τ, is the x-intercept of the fictitious line. However, it is important to note that the form of the input is a step function at *t* =0. Therefore, the time constant measured off of the oscilloscope is measured from the instant in time when the step voltage is applied. In other words, on the oscilloscope, *t* =0 is defined as the point when the step voltage is applied.

AWT conducted an experiment to determine the constants in equation 6.8.1. Ten arbitrary voltages were applied to the so-called process dynamics block of the Educational Servo. From the ten input voltages, ten measurements were taken of x-intercepts and the slope of the response curve. The data is given in appendix C. The average value of the process dynamics gain, *K*, and the time constant, τ, were calculated. Anomalous data was removed and attributed to bad measurements off of the oscilloscope. AWT's mathematical model of the process dynamics of the position control function of the Educational Servo is presented as follows

$$G_p(s) = \frac{49.2}{s \cdot (0.231s + 1)} \qquad [6.8.8]$$

The units of *K* are 1/s and the unit of τ is sec.

6.9 Mathematical Model Validation

In theory, a mathematical model of the process dynamics of the system allows AWT to predict the response of the position control system of the Educational Servo. For instance, on the Educational Servo, an input of a reference angle of 80^o corresponds to inputting 8 volts into the system. The block diagram representation of the positional control system of the Educational Servo may then be used to solve for the response of the system to 8 volt input; the Matlab affiliated program, Simulink, was specifically designed for this. With Simulink, the block diagram can be entered as shown in figure 46

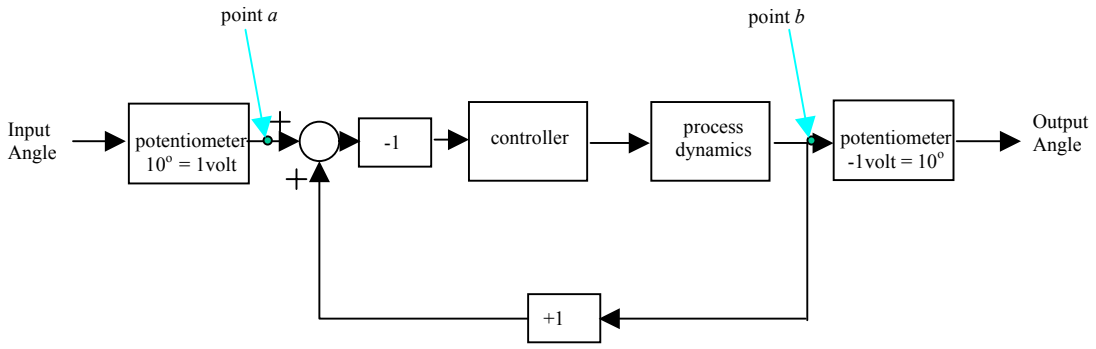

Figure 46. Position Control Model for Educational Servo

The transfer function of the process dynamics is input directly as seen in equation 6.8.8. For simplicity, let the controller be a proportional controller with C= 1.0498; a proportional controller is reviewed in Appendix D. With Simulink, the response of the output of the output angle and/or the output voltage to the potentiometer can be simulated for any given input. AWT chose to simulate the output voltage that feeds the output potentiometer versus the input voltage that comes from the input potentiometer. On figure 46, this is the response at point *b* to an input at point *a*. This simulation was chosen because the voltage at point *a* and *b* can be directly displayed on a digital oscilloscope for comparison. The result of the Simulink simulation is presented in figure 47.

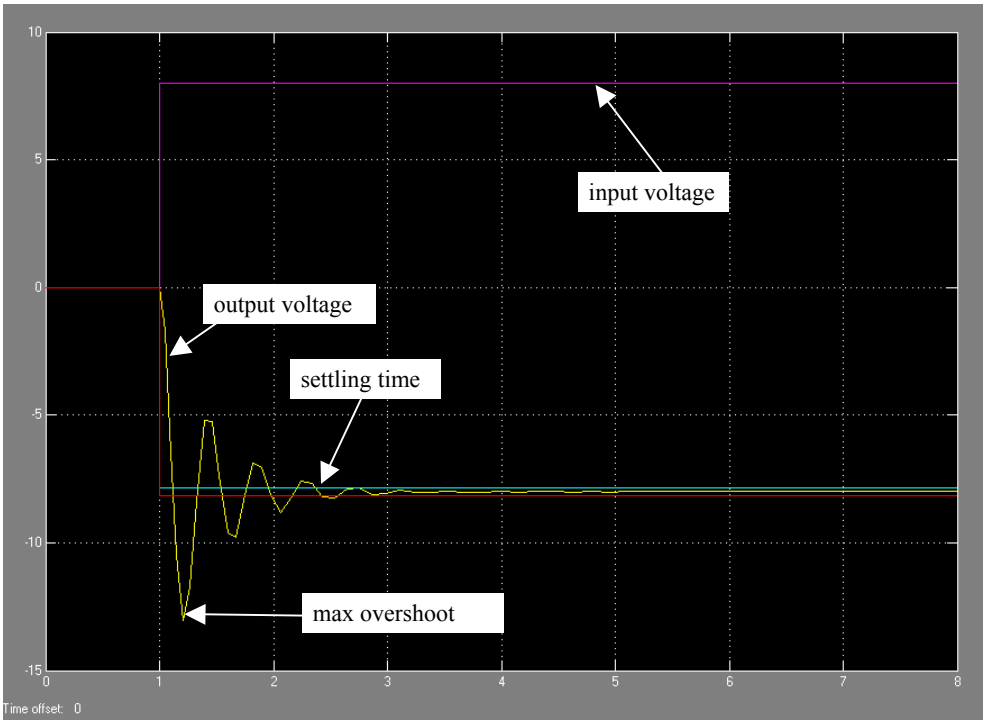

Figure 47. Simulated response

Before AWT can claim that the simulation exactly represents the real-life process, the simulation must be compared with the oscilloscope display of the response of the output voltage to an input voltage of 8 volts. The same parameters that were in the simulation must be mirrored in the experiment. The setup of the experiment on the face of the Educational Servo is shown in figure 48 below.

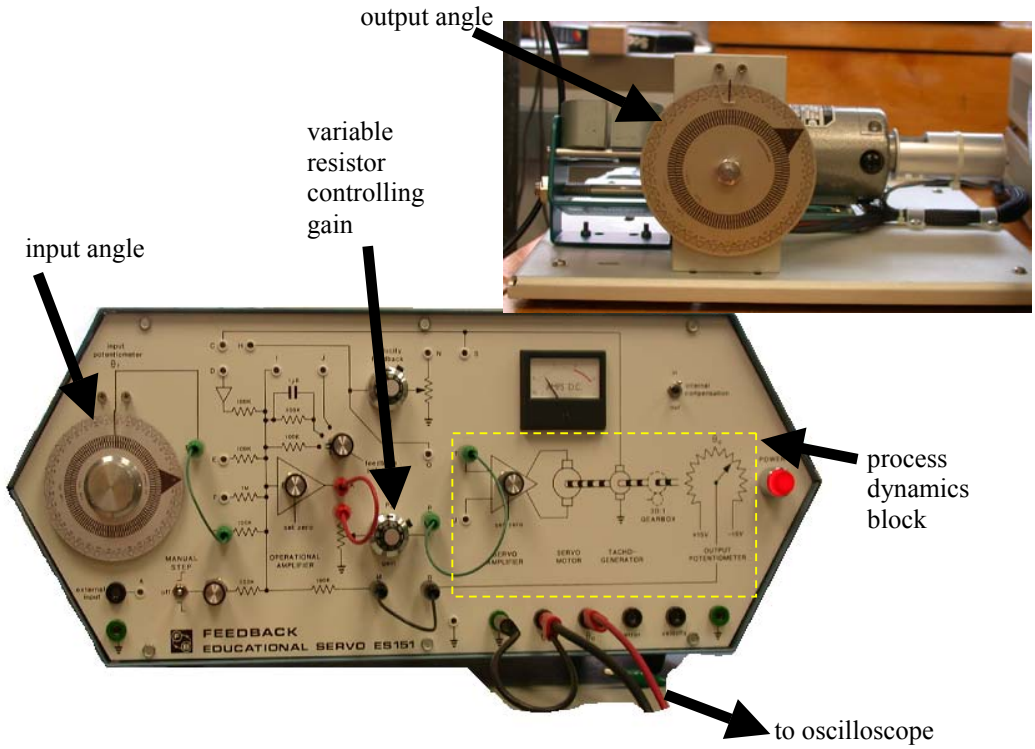

Figure 48. Setup of Validation Experiment

On figure 48, there is an arrow pointing to a variable resistor that controls the gain of the proportional controller. According to equation D.2 in Appendix D, setting the resistance to 4.98 KΩ provides a proportional control of 1.0498. Setting the input angle to 80^{o} provides an input voltage of 8 volts. The response of the output voltage to the input 8 volts is shown in figure 49. Remember that the response of the output voltage to the input voltage is representative of the response of the output angle to the input angle.

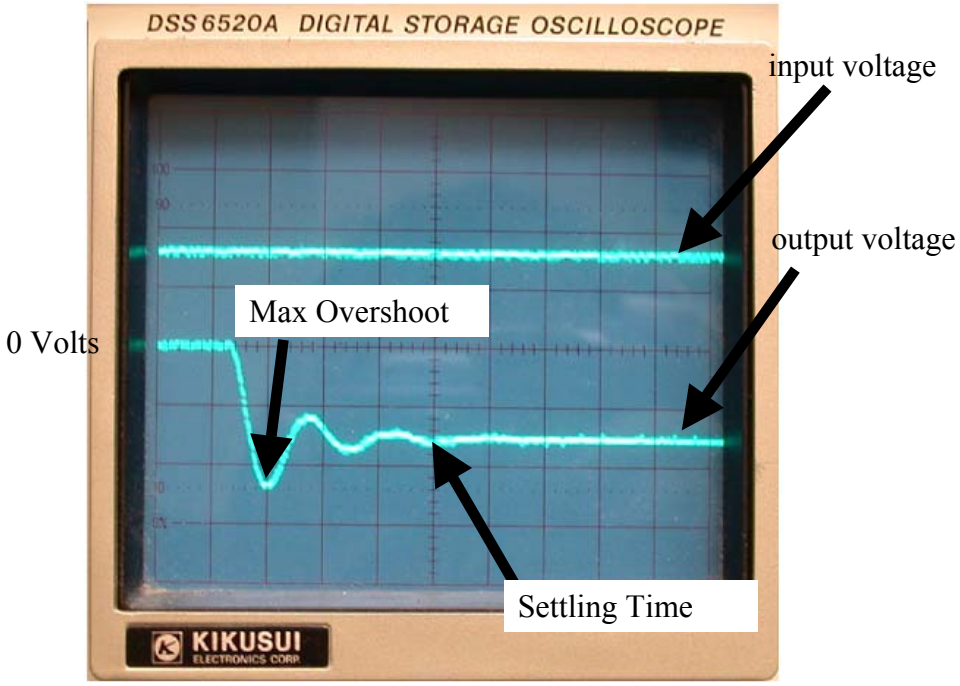

Figure 49. Actual Response

A comparison of the actual response displayed on the oscilloscope to the simulated response with Simulink shows that the mathematical model of the position control system of the Educational Servo is reasonable. The difference between the settling times of the two responses is around 0.5 sec and the difference between the maximum overshoot is 1 volt.

AWT has demonstrated the angular position control of the Educational Servo. Future groups can follow a similar process and formulate a mathematical model of the rotation control of the Educational Servo. Furthermore, future groups can design an implementation scheme utilizing the angular position control and rotation control characteristics in the wing-stabilator model. AWT suggests that the position control feature of the Educational Servo may be used to control the wing sweep; while the rotational control feature could be used in conjunction with a crank-shaft to oscillate a

flap. However, depending on the implementation scheme of future groups, the mathematical model of the educational servo developed by AWT must be modified.

6.10 Digital Control System

The fundamental difference between a digital control system and an analog control system is that a digital system utilizes digital signals and a digital computer to control a process [19]. The primary difference is illustrated below in figure 50.

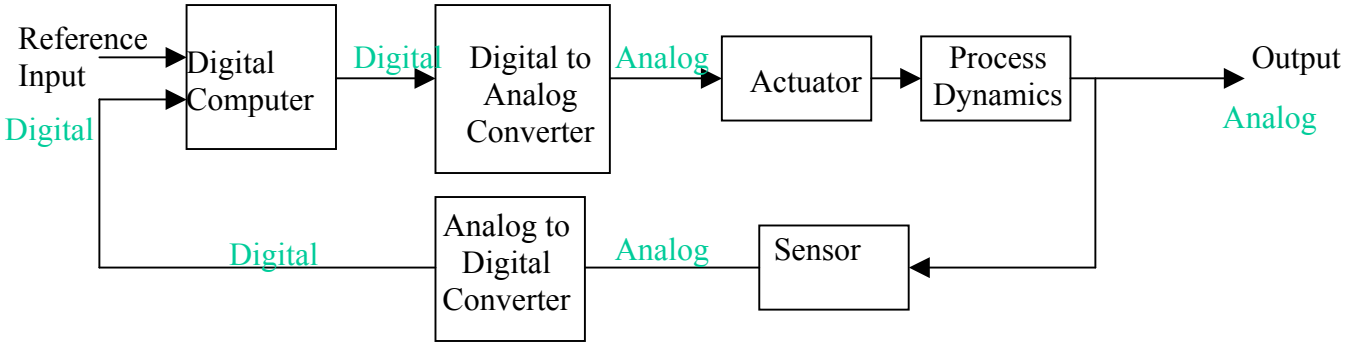

Figure 50. Digital Control System

Notice that the digital system shown above is a modification of the controller section of the analog system in figure 25. Instead of designing an amplifying circuit, as seen in figure 23, to provide the transfer function necessary to control the process, a computer is used. The benefit of the digital controller is that an extensive knowledge of electronic circuits is not required; however one must be proficient in Control Theory and programming.

6.10.1 Digital-to-Analog and Analog-to-Digital Converters

The signals input into a computer and output signals of the computer are in digital form. An analog-to-digital converter must be used to change the analog voltage signal to a digital signal for the computer to use. Furthermore, when the computer has computed and output the necessary control actions, a digital-to-analog converter must be used to

convert the digital signal of the computer to an analog voltage signal to control the process.

7.0 Progress

Time constraints have limited the progress of AWT to so-called paper designs. The following sections will detail the work accomplished by Active Wing Technologies over the course of the Summer 2002 semester and will also provide suggestions for future work to subsequent research groups.

7.1 Work Completed

The first half of the semester was dedicated towards background research and finding information on supplies such actuators, controllers, and control surface materials. Completed work is described below.

Wing Stabilator Model

Active Wing Technologies, in conjunction with Dr. Stearman and Sean Hinze, had the model reassembled and placed in room 319 of the W.R. Woolrich Laboratories building (WRW). The model and subsystems include:

- Root wing-stabilator
- Hydraulic Servo Controller
- High-pressure hydraulic pump with hoses for hydraulic fluid and one pneumatic pressure line
- F-111 model wing
- Nose and stabilator wedges
- F-111 model stabilator (never recovered from storage)

Components of the hydraulic system were recovered from Austin Hydraulics courtesy of Sean Hinze. The system was placed on the primary mount and secured by bolts. Since

Active Wing Technologies has decided to change the power supply system on the advice of Dr. Stearman, Austin Hydraulics was paid for their services and service was cancelled.

Research

Naoki Sato investigated limited cycle oscillation, system identification, increasing the maximum lift coefficient, and actuator power supplies (hydraulic system, piezoelectric system, and magnetic shape memory material.) Most of the information about LCO and system identification was provided by the Active Wing Group's paper. Information about the actuator power supply was found in various web sites. During the second half of the semester, Naoki researched means of increasing the lift coefficients of fighter aircrafts. Dr. Stearman noted that Israel had recently discovered ways of increasing lift drastically when compared to the United States' capabilities. He centered his research on Israel's findings on increasing lift of fighter aircrafts.

Basil Philip studied methods of implementing control surfaces on the F-111 wing model. He sought information from such aeroelasticity experts as Dr. Ronald Stearman of the UT Aerospace Department and Frank Wise, also of the UT Department. Both individuals provided guidance, background information, and numerous additional sources of technical information. He later developed designs in AutoCAD as possible schemes of constructing and implementing control surfaces.

David Fuentes researched analog and digital control systems. David was able to operate the Educational Servo, which he eventually determined was an analog controller. He developed a mathematical model of the position control feature of the Educational Servo. The process in formulating the analytical model will be value for future groups to optimize controller designs.

AutoCAD Schematic

As an aid to future groups, members of Active Wing Technologies and the Wavelet Group transferred actual size drawings into AutoCAD. This schematic will prove useful in the continued reconstruction and refitting of the model. Furthermore, digitizing the schematics has distinct advantages over the deteriorating qualities of the paper form of storing the schematics. Digital copies of the AutoCad drawings will be handed in with the project notebook.

7.2 Incomplete Endeavors

Some things are simply beyond our control or so unexpected that they can provide significant barriers to progress. Due to setbacks and complications, Active Wing Technologies has realized that some of the goals are impossible in such short time. This section will provide an overview of Active Wing Technologies unsuccessful activities:

- The stabilator for the model was never found. It is possible that it could still be in a UT storage facility. If the stabilator is unable to be found, a new stabilator must be designed and constructed.
- Active Wing Technologies never decided on a power supply to provide for wing sweep and control surface pivoting. Several systems have been well researched and a is left for future groups.
- Control surfaces were not implemented on the F-111 model wing. The research provided in this report is a solid foundation for future groups to initialize control surface implementation.

- Wind tunnel testing was beyond reach for Active Wing Technologies and is a future goal for future groups continuing active aeroelastic wing and LCO studies.
- The Educational Servo was originally thought to be a digital system. However, the Educational Servo was found to be an analog system and Active Wing Technologies was successful understanding its modes of operation. However, ways of relating the system to the model is still to be done.

7.3 Recommendations For Future Groups

AWT's provides the following recommendations for future groups.

Actuator Power Supply System

Research has shown the maximum frequency range of Bolding's analog system was 56Hz. AWT suspects that a higher frequency range will be necessary to utilize control surfaces in the active wing. Before deciding on a power supply system, future groups must do an analytical study to obtain a conservative estimate of the frequency range required of control surfaces. The final choice of the actuator power supply must take into account its ability to perform in the frequency range required by the control surfaces.

Control Electronics

AWT has demonstrated the angular position control and rotational speed control of shaft on the motor of the Educational Servo. Future groups should consider using the angular position control feature of the Educational Servo as a mechanism to control the wing sweep angle of the wing-stabilator model. A crankshaft may be used to convert the

rotational motion of the shaft on the DC motor to oscillatory motion to drive the flaps in future designs of the active wing. However, AWT recommends that a digital control system should be utilized to implement the control laws for optimizing the use of the oscillating motion of the flaps. The use of analog circuitry to implement complex control laws is outdated.

The formulation of analytical models of the processes involved with the active wing is vital. Mathematical models of the control processes related to the active wing allow optimal controllers to be designed using either the root locus method or bode plots.

8.0 Cost Analysis

Since Active Wing Technologies decided to abandon the hydraulic system as the power supply for the wing model, an amount of a hundred dollars was paid to Austin Hydraulics in order to settle for their troubles. As of mid-semester, Active Wing Technologies has not incurred any charges at the moment.

The projected cost of the digital controller and two converters is $100. The software to program the digital controller will be the most expensive. However, Labview is a well-designed programming environment used by faculty at WRW. Use of the current Labview licenses held by faculty would save future group's resources.

In spite of the fact that the MSM based actuator manufactured by AdaptaMat Ltd. is too costly ($5000) for the budget of current design teams, future groups should not give up on the MSM actuator. The MSM actuator is still in early stages of production. Advances in the production capability of AdaptaMat Ltd are sure to lower the prices for future groups.

9.0 Schedule

Schedule	
June 10–14	Met with Sean Hinze and Dr. Stearman Tentative division of the project work Basil Philip– Team leader & Hydraulics David Fuentes– Avionics Naoki Sato– Mechanics Looked over wing drawings
June 17–21	Dr. Stearman went to Austin Hydraulics Decided to go with a new modern power supply Found references for power supplies Decided to work on digital control system Reviewed last years work and 1978 masters thesis
June 24–28	Spoke to Frank Wise about the power supply Requirements and specifications for the power supply Pressure – 1000psi Volumetric Flow Rate at – 7.082 cc/s = .007082 Liter/s
July 1–5	Spoke to Frank Wise about a new possibility for a power supply Read paper on Magnetic Shape Memory material
July 8–12	Practiced midterm oral presentation
July 15–19	Met with Dr. Juan Senent to discuss possible implementation schemes for digital controllers
July 22–26	Chose the main topics that will be presented on the final oral presentation Basil– Control surface implementation David- Analog controller for wing sweep position control Naoki– Methods to increase the maximum lift coefficient
July 29–August 2	Worked on final project

August 5–9	Practiced final oral presentation
August 12–16	Finish touches on final paper

References

[1] Bolding, Randall "The Design, Analysis, and Testing of a Wind Tunnel Model with Active Aerodynamic Controls for Flutter Suppression, " University of Texas at Austin, Austin, TX, 1978.

[2] Prosser, Robin, Hinze, Sean, Mears, Paul, Tobar, Francisco,and Benito III, Hipolito, "Assembly and Control Modeling of an Active Variable Geometry Wing," Active Wing Group, Austin, TX, May. 2002.

[3] "High Lift Devices," Dave Esser, 1998, http://comm.db.erau.edu/esser/wp1.html

[4] "Anatomy of a STOL Aircraft: Designing a Modern Short Take-Off and Landing Aircraft," Chris Heintz, http://www.zenithair.com/stolch801/design/design.html

[5] "Aircraft Design: Synthesis and Analysis," Desktop Aeronautics http://adg.stanford.edu/aa241/AircraftDesign.html

[6] "High-incidence Airfoil Aerodynamics Improvement by Leading-Edge Oscillating Flap," F.B.Hsiao, P.F.Liang, C .Y.Hunan, Jurnal of Aircraft Vol35, No.3

[7] Sandford, Maynard C., Abel, Irving, and Gray, David L., "Development and Demonstration of a Flutter-Suppression Using Active Controls," NASA, L-10446, Washington, D.C., December 1975.

[8] Nissim, El: Flutter Suppression Using Active Wing Controls Based on the Concept of Aerodynamic Energy. NASA TN D-6199, 1971.

[9] Hull, David G., "Static Stability and Control," *Introduction to Airplane Flight Mechanics*, The University of Texas at Austin, Texas, 2001, pp. 7:1-7:29.

[10] "Hydraulic System," Mobil Crane Club, http://www.crane-club.com/lecture/oilpressure.htm

[11] "Hydraulic System," The Vintage Ford Tractor Resource, http://members.aol.com/naa60512/hyd.htm

[12] "Piezoelectric Effect," Infoplease.com, http://www.infoplease.com/ce6/sci/A0839004.html

[13] "Smart Material," Esmart, August 21. 2001 http://www.cs.ualberta.ca/~database/MEMS/sma_mems/smrt.html

[14] "Piezoelectric Transducers," Industrial Technology http://www.industrialtechnology.co.uk/lambda.htm

[15] "Magnetic Shape Memory Alloys," Helsinki University of Technology, September 10. 2001
http://www.fyslab.hut.fi/epm/heusler/

[16] "Smart Actuator Materials," AdaptaMat,
http://www.adaptamat.com/materials.html

[17] Cogdell J.R., "Analog Electronics," *Foundations of Electronics*, 1st ed, Prentice Hall, New Jersey, 1999, pp.194-277.

[18] Haykin, Simon, Veen, Barry V., "Partial Fraction Expansions," *Signals and Systems*, John Wiley & Sons, New York, 1999, pp. 671-675.

[19] Bishop, Robert "Digital Control Systems," *Modern Control Systems*, 9th ed, Prentice Hall, New Jersey, 2001, pp. 743-784.

Appendix A

Electrical Circuit Schematic of Educational Servo System

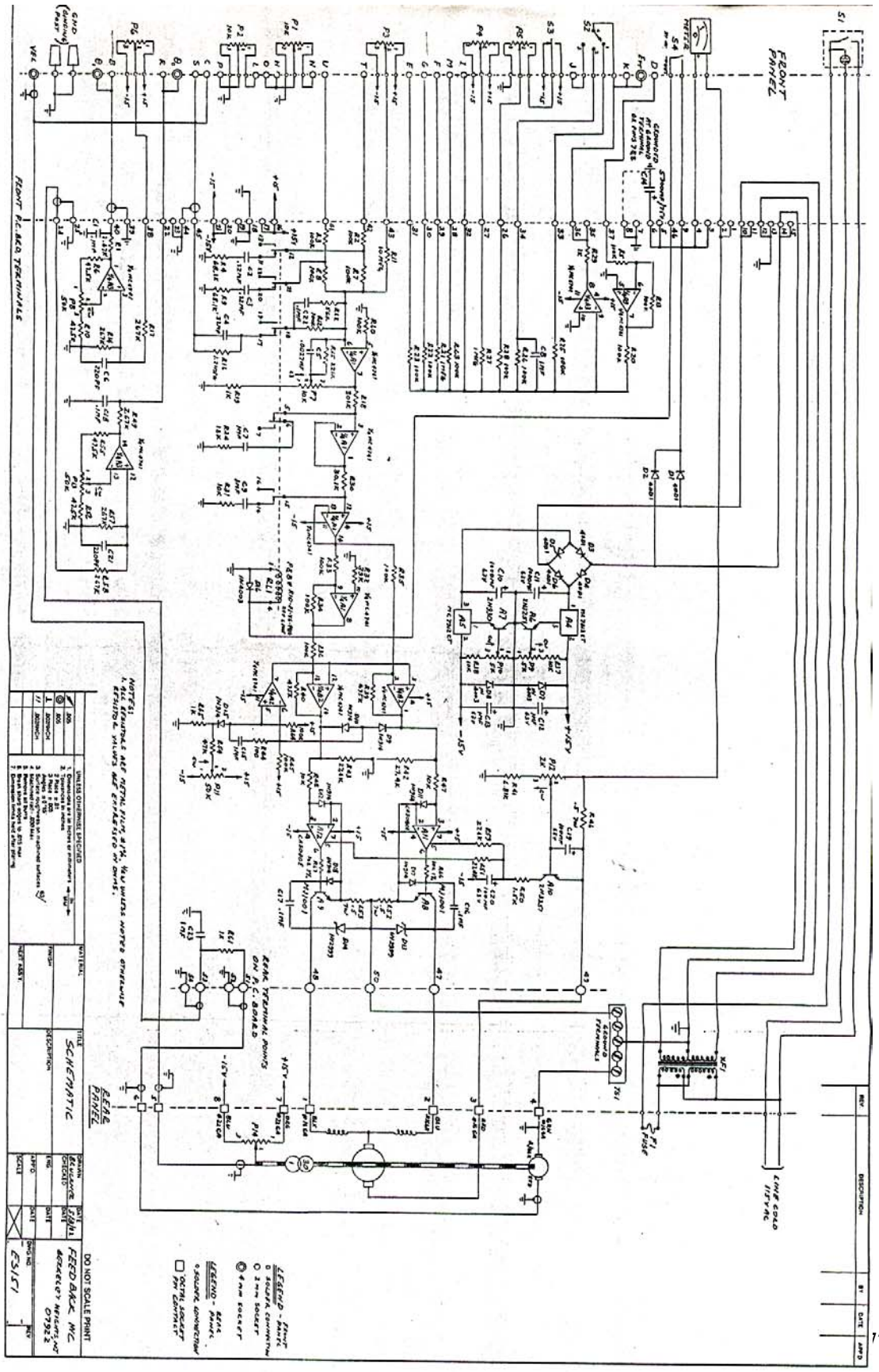

Appendix B

Important Laplace Transform Pairs [19]

$f(t)$	$F(s)$
Step function, $u(t)$	$\frac{1}{s}$
e^{-at}	$\frac{1}{s+a}$
$\sin \omega t$	$\frac{\omega}{s^2+\omega^2}$
$\cos \omega t$	$\frac{s}{s^2+\omega^2}$
t^n	$\frac{n!}{s^{n+1}}$
$f^{(k)}(t) = \frac{d^k f(t)}{dt^k}$	$s^k F(s) - s^{k-1} f(0^-) - s^{k-2} f'(0^-) - \ldots - f^{(k-1)}(0^-)$
$\int_{-\infty}^{t} f(t)dt$	$\frac{F(s)}{s} + \frac{1}{s}\int_{-\infty}^{0} f(t)\,dt$
Impulse function $\delta(t)$	1
$e^{-at} \sin \omega t$	$\frac{\omega}{(s+a)^2+\omega^2}$
$e^{-at} \cos \omega t$	$\frac{(s+a)}{(s+a)^2+\omega^2}$
$\frac{1}{\omega}[(\alpha-a)^2+\omega^2]^{1/2} e^{-at} \sin(\omega t+\phi)$, $\phi = \tan^{-1}\frac{\omega}{\alpha-a}$	$\frac{s+\alpha}{(s+a)^2+\omega^2}$
$\frac{\omega_n}{\sqrt{1-\zeta^2}} e^{-\zeta\omega_n t} \sin \omega_n\sqrt{1-\zeta^2}\, t, \zeta < 1$	$\frac{\omega_n^2}{s^2+2\zeta\omega_n s+\omega_n^2}$
$\frac{1}{a^2+\omega^2} + \frac{1}{\omega\sqrt{a^2+\omega^2}} e^{-at} \sin(\omega t-\phi)$, $\phi = \tan^{-1}\frac{\omega}{-a}$	$\frac{1}{s[(s+a)^2+\omega^2]}$
$1 - \frac{1}{\sqrt{1-\zeta^2}} e^{-\zeta\omega_n t} \sin(\omega_n\sqrt{1-\zeta^2}\, t+\phi)$, $\phi = \cos^{-1}\zeta, \zeta < 1$	$\frac{\omega_n^2}{s(s^2+2\zeta\omega_n s+\omega_n^2)}$
$\frac{\alpha}{a^2+\omega^2} + \frac{1}{\omega}\left[\frac{(\alpha-a)^2+\omega^2}{a^2+\omega^2}\right]^{1/2} e^{-at} \sin(\omega t+\phi)$, $\phi = \tan^{-1}\frac{\omega}{\alpha-a} - \tan^{-1}\frac{\omega}{-a}$	$\frac{(s+\alpha)}{s[(s+a)^2+\omega^2]}$

Appendix C

Data from Process Dynamics Modeling Experiment

Vin (volts)	Vin K (volts/sec)	K (1/sec)	τ(sec)
0.219	10	45.66210046	0.28
0.16	8.333333333	52.08333333	0.36
0.2	10	50	0.2
-0.65	-27.7777778	42.73504274	0.14
-0.17	-8.62068966	50.70993915	0.28
0.18	10	55.55555556	0.24
0.6	29.41176471	49.01960784	0.15
-0.55	-26.3157895	47.84688995	0.16
-0.05	-20	anomaly	0.5
0.26	30	anomaly	0.14
		49.20155863	0.231

Appendix D

This section provides several types of analog controllers and derivations of their transfer functions.

Proportional Controller

The proportional controller, commonly referred to as a P controller, provides the transfer function of the from listed below

$$G_c = C \qquad [D.1]$$

The proportional controller is the simplest type of controller; its transfer function may be implemented with the op amp circuit shown in figure 51 below

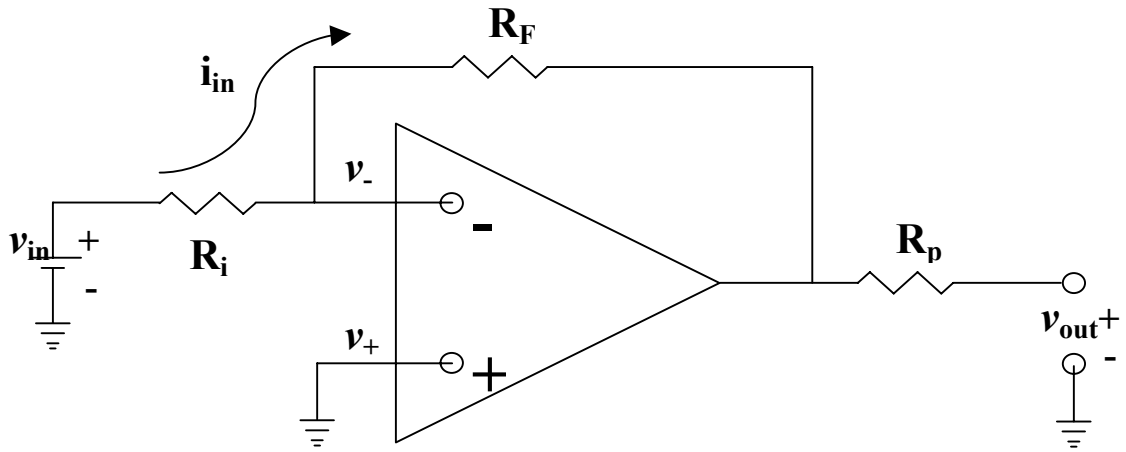

Figure 51. Proportional Controller

Assume that the input voltage, V_{in}, is representative of the error between the input reference value and the actual value. Analysis of the circuit in figure 51 is similar to the inverting amplifier analysis from Section 6.3. It is left as an exercise to the reader to show that the transfer function between in the input voltage and the output voltage, V_{out}, is as follows

$$\frac{V_{out}(s)}{V_{in}(s)} = -\left(\frac{R_F}{R_i} + \frac{R_p}{R_i}\right) \qquad [D.2]$$

As shown in equation D.2, the ratio of the resistors provides the gain of the controller. If the negative sign in the transfer function is not desired an inverting amplifier may be utilized.

Proportional-Derivative Controller

The proportional-derivative controller is commonly referred to as the PD controller. A PD controller provides a transfer function of the form below

$$G_c = C \cdot (s + a) \qquad [D.3]$$

The transfer function of a PD controller may be implemented with the circuit shown below in figure 52.

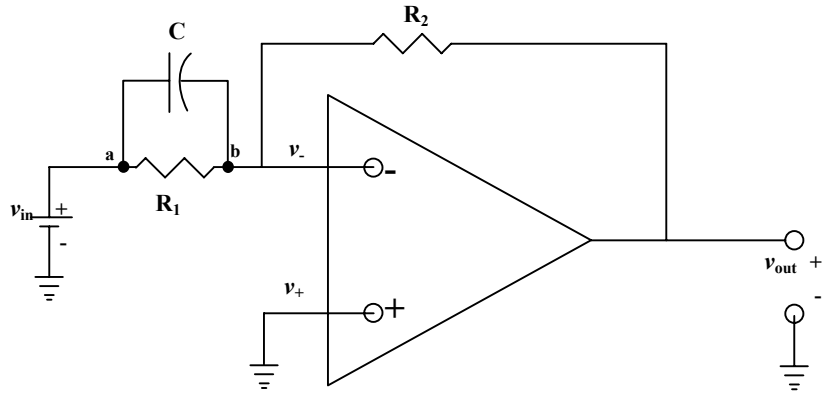

Figure 52. PD Controller [19]

Let the input voltage, V_{in}, be representative of the error between the desired value and the actual value. Recall the relationship between the current through a capacitor and the resulting voltage across the capacitor is given be the following equation

$$i_c = C\frac{dv_c}{dt} \qquad [D.4]$$

Using node voltage analysis we can write an equation summing the currents at node *b*

$$\frac{v_b - v_{out}}{R_2} = \frac{v_{in} - v_b}{R_1} + C\frac{dv_c}{dt} \qquad [D.5]$$

Recall from section 6.3 that the voltage at the negative input terminal to the op amp is approximately zero if the positive terminal is grounded. Equation D.5 may be simplified as follows

$$\frac{-v_{out}}{R_2} = \frac{v_{in}}{R_1} + C\frac{dv_c}{dt} \qquad [D.6]$$

Furthermore, because $v_- \approx 0$, the sum of the voltages from the input voltage to the voltage across the capacitor equals zero

$$v_{in} - v_c = 0 \Rightarrow v_{in} = v_c \qquad [D.7]$$

Combining equations D.6 and D.7 yield a differential equation relating the input voltage to the output voltage

$$\frac{-v_{out}}{R_2} = \frac{v_{in}}{R_1} + C\frac{dv_{in}}{dt} \qquad [D.8]$$

Applying the Laplacean operator to equation D.8 and simplifying yields a transfer function of the form in equation D.3

$$\frac{-1}{R_2} \cdot V_{out}(s) = \frac{1}{R_1} \cdot V_{in}(s) + s \cdot C \cdot V_{in}(s) \qquad [D.9]$$

$$\frac{V_{out}(s)}{V_{in}(s)} = -\left(\frac{R_2}{R_1} \cdot + R_2 \cdot C \cdot s\right) = -R_2 \cdot C \cdot \left(\frac{1}{R_1 \cdot C} + s\right) \qquad [D.10]$$

Proportional-Integrating Controller

The proportional-integrating controller is commonly referred to as the PI controller. A PI controller provides a transfer function of the form below:

$$G_c = \frac{C \cdot (s + a)}{s} \qquad [D.11]$$

The transfer function of a PI controller may be implemented with the circuit shown below in figure 53.

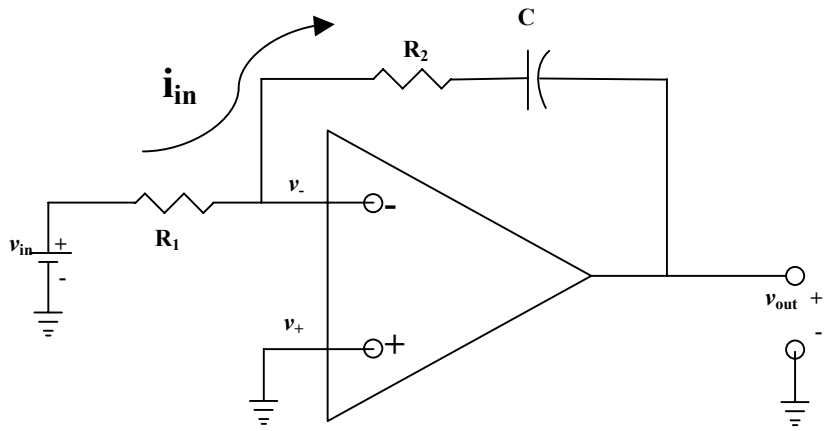

Figure 53. PI Controller [19]

For the same reason as in section 6.3, $v_- \approx 0$. Because the input voltage at the negative terminal of the op amp is approximately zero, the sum of the voltages across R_2, the capacitor, and the output voltage is zero. Furthermore, i_{in} is the same current that passes through R_1, R_2, and C

$$i_{in}R_2 + v_c + v_{out} = \frac{v_{in}}{R_1}R_2 + v_c + v_{out} = 0 \qquad [D.12]$$

Taking the derivative of equation D.12 yields the following result:

$$\frac{d}{dt}\left(\frac{v_{in}}{R_1}R_2 + v_c + v_{out} = 0\right) \Rightarrow \frac{d}{dt}\left(v_{in}\frac{R_2}{R_1}\right) + \frac{dv_c}{dt} + \frac{dv_{out}}{dt} = 0 \qquad [D.13]$$

Equation D.13 may be combined with the defining equation of a capacitor, as shown in equation D.4. The result is a differential equation relating the input voltage and the output voltage

$$\frac{R_2}{R_1}\cdot\frac{dv_{in}}{dt}+\frac{v_{in}}{R_1\cdot C}+\frac{dv_{out}}{dt}=0 \qquad [D.14]$$

Once again the Laplace operator is applied to the differential equation. The simplified from of the transfer function between the input and output voltage resembles the form in equation [D.11]

$$s\cdot V_{in}(s)\cdot\frac{R_2}{R_1}+\frac{1}{R_1\cdot C}\cdot V_{in}(s)+s\cdot V_{out}(s)=0 \qquad [D.15]$$

$$\frac{V_{out}(s)}{V_{in}(s)}=-\left(\frac{R_2\cdot C\cdot s+1}{R_1\cdot C\cdot s}\right)=-\frac{R_2}{R_1}\left(\frac{s+\dfrac{1}{R_2\cdot C}}{s}\right) \qquad [D.16]$$

Proportional-Integrating-Derivative Controller

A proportional-integrating-derivative controller is typically called a PID controller. The defining transfer function of a PID controller is of the form presented below

$$G_c=C\frac{(s+a)(s+b)}{s} \qquad [D.17]$$

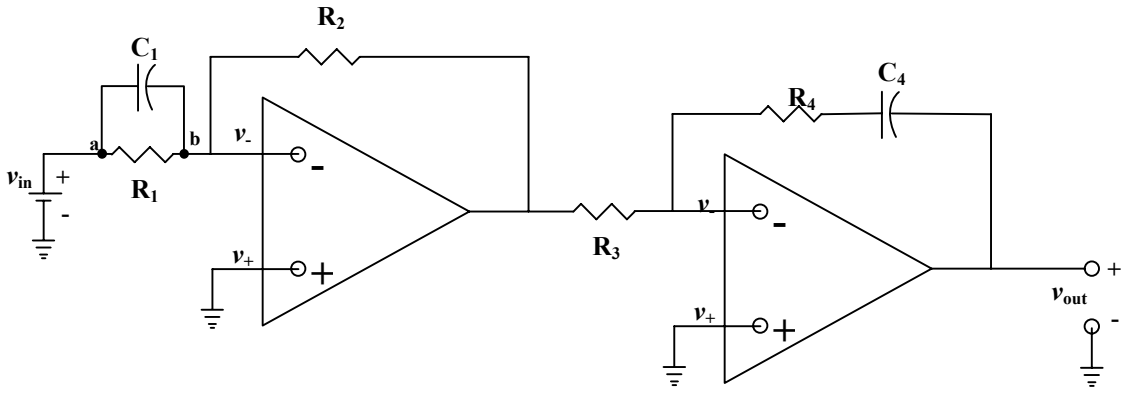

Figure 54. PID controller

The transfer function of the PID controller may be obtained from a superposition of the transfer functions of a PI and a PD controller. First start with the transfer function of the PD controller on the left

$$V_{pd}(s) = -\left(\frac{R_2}{R_1} \cdot + R_2 \cdot C_1 \cdot s\right) \cdot V_{in}(s) \qquad [D.18]$$

The output of the PD controller is the input of the PI controller on the right:

$$V_{out}(s) = -\left(\frac{R_4 \cdot C_4 \cdot s + 1}{R_3 \cdot C_4 \cdot s}\right) \cdot V_{pd}(s) = \left(\frac{R_4 \cdot C_4 \cdot s + 1}{R_3 \cdot C_4 \cdot s}\right)\left(\frac{R_2}{R_1} \cdot + R_2 \cdot C_1 \cdot s\right) \cdot V_{in}(s) \quad [D.19]$$

The resulting transfer function is the ration of the output voltage to the input voltage. Further the transfer function may be shown to be of the form in Equation D.17:

$$\frac{V_{out}(s)}{V_{in}(s)} = \frac{\left(R_4 \cdot C_4 \cdot s + 1\right)\left(\frac{R_2}{R_1} \cdot + R_2 \cdot C_1 \cdot s\right)}{R_3 \cdot C_4 \cdot s} = \frac{R_4 \cdot R_2}{R_3} \cdot \frac{\left(s + \frac{1}{C_4 R_4}\right)\left(s + \frac{1}{C_1 R_1}\right)}{s} \qquad [D.20]$$